UC San Diego

UC San Diego Previously Published Works

Title

Coordinated Management of Mobile Charging Stations and Community Energy Storage for Electric Vehicle Charging

Permalink

https://escholarship.org/uc/item/3qx173v4

Journal

Applied Energy, 393

ISSN

0306-2619

Authors

Taşcıkaraoğlu, Akın

Beyazıt, Muhammed Ali

Kleissl, Jan

et al.

Publication Date

2025-09-01

DOI

10.1016/j.apenergy.2025.126066

Copyright Information

This work is made available under the terms of a Creative Commons Attribution License, available at https://creativecommons.org/licenses/by/4.0/

Peer reviewed

eScholarship.org Powered by the California Digital Library
University of California

Coordinated Management of Mobile Charging Stations and Community Energy Storage for Electric Vehicle Charging

Akın Taşcıkaraoğlu[1,2,*], Muhammed Ali Beyazıt[1], Jan Kleissl[3], Yuanyuan Shi[2]

[1] Department of Electrical and Electronics Engineering, Muğla Sıtkı Koçman University, Muğla, Türkiye

[2] Electrical and Computer Engineering Department, University of California San Diego, California, USA

[3] Center for Energy Research, University of California San Diego, California, USA

* *akintascikaraoglu@mu.edu.tr*

Abstract

Widespread adoption of electric vehicles (EVs) largely relies on the availability of a charging infrastructure. However, the significant installation costs, need for appropriate locations, congestion and lengthy queues at public fixed charging station (FCS), and the potential strain on the grid hinder the expansion of the charging station network, particularly in urban areas. To address these shortcomings associated with FCSs, mobile charging stations (MCSs) can be used as a supplementary solution. To this end, an optimization framework that incorporates FCSs and MCSs is proposed to meet the spatiotemporally distributed EV charging demands. A community energy storage system (CESS) is integrated into the system to enhance the flexibility and increase the use of renewable energy in EV charging. When the EV charging requests are received, the proposed framework determines the optimal charging technology and location for each charging demand by taking charging site and time preferences of EV users into account. The simulation studies and comparative analyses demonstrate that the proposed framework enhances benefits for both the operators and EV users, achieving a 90% reduction in carbon emissions and reducing waiting times at FCSs to zero. Further analyses confirm its effectiveness across various conditions, leading to substantial reductions in emissions and costs, particularly in larger systems. Compared to an MCS scheduling method based on EV clustering, the proposed framework achieves lower emissions while slightly increasing battery degradation.

Keywords: Carbon emission minimization, community energy storage, electric vehicle charging station, mobile charging station.

Nomenclature

A. Indices

e	Electric vehicles (EVs)
i, j	Nodes
m	Mobile charging stations (MCSs)
t, tt	Time periods

B. Sets

E	EVs, e $\in E$
M	MCSs, $m \in M$
N	Nodes, $i, j \in N$
$N^{1,2}$	Depot nodes, $i, j \in N^{1,2}$
N'	Fixed charging station (FCS) nodes, $i, j \in N'$
R	Routes, $(i, j) \in R$
T	Time periods, t $\in T$
T'	Time periods for minimum carbon emission period, $t \in T'$

C. Parameters

$\mathrm{arr}_{e,t}^{\mathrm{EV}}$	Binary parameter; 1 if EV e arrives the designated node in time period t, else 0
C_i^{fx}	Number of fixed chargers for FCS at node i
C_m^{MCS}	Number of chargers on MCS m
$D_{i,j}$	Distance between nodes i, j (km)
DoD	Deep discharge value of MCS and CESS batteries
N_{cycle}	Battery cycle life of CESS and MCSs
ord_t	Order value of each time period t
$\mathrm{place}_{i,e}$	Matrix to determine EV nodes
$\mathrm{SOE}^{\mathrm{CESS,ini}}, \mathrm{SOE}^{\mathrm{CESS,max}}, \mathrm{SOE}^{\mathrm{CESS,min}}$	Initial/maximum/minimum SOE value of CESS (kWh)
$\mathrm{SOE}_e^{\mathrm{EV,ini}}$	Initial SOE value of EV e (kWh)
$\mathrm{SOE}^{\mathrm{MCS,ini}}, \mathrm{SOE}^{\mathrm{MCS,max}}, \mathrm{SOE}^{\mathrm{MCS,min}}$	Initial/maximum/minimum SOE value of MCSs (kWh)
$\mathrm{SOE}_e^{\mathrm{req}}$	Requested SOE for EV e at the completion of the charging process (kWh)
SV	Salvage value of CESS and MCSs batteries
$\Im_e^{\mathrm{arr}}$	Arrival time of EV e
t^0, t^{end}	Charging service start/end time
ΔT	Determined time period
$\eta^{\mathrm{ch/dch}}, \eta^{mcs}$	Charging/discharging efficiency of CESS and MCSs
η^{fx}	Charging efficiency of FCS
λ_t^{CO2}	CO_2 price in time period t
$\lambda^{\mathrm{CESSdeg}}, \lambda^{\mathrm{MCSdeg}}$	Battery degradation cost of CESS and MCSs ($/kWh)
λ^{miss}	Penalty cost for each EV missed by the MCSs
λ^{wait}	Penalty cost due to waiting time

σ^{way}	Energy consumption of MCSs for travel (kWh/km)
π_{unit}	Battery purchase cost of CESS and MCSs ($/kWh)
$\mathfrak{B}$	A large positive value
$\mathcal{R}^{\text{CESS}}$	Charging/discharging rate of CESS (kW)
$\mathcal{R}_i^{\text{fx}}$	Charging rate of FCS i (kW)
$\mathcal{R}^{\text{ch,MCS}}, \mathcal{R}^{\text{dch,MCS}}$	Charging/discharging rate of MCSs (kW)
$\mathcal{R}^{\text{MCS,tot}}$	Total discharging rate of MCSs (kW)
$\mathcal{T}_{i,j}^{\text{way}}$	Travel time from i to j

D. Real Variables

$E_{m,i,j,t}^{\text{way}}$	Energy consumed by MCS m while traveling from i to j in time period t (kWh)
$P_{i,e,t}^{\text{ch,fx}}$	Charging power of EV e at FCS i in time period t (kW)
$P_{m,i,t}^{\text{ch,MCS}}$	Charging power delivered by MCS m at depot i in time period t (kW)
$P_{m,i,e,t}^{\text{dch,MCS}}$	Discharging power of MCS m to charge EV e at node i during time period t (kW)
$P_t^{\text{CESS}\to\text{FCS}}$	Power from CESS to FCSs at time period t
$P_t^{\text{ch,CESS}}, P_t^{\text{dch,CESS}}$	Charging/discharging power of CESS during time period t (kW)
$P_t^{G\to\text{CESS}}, P_t^{G\to\text{FCS}}, P_t^{G\to\text{MCS}}$	Powers from grid to CESS/FCSs/MCSs at time period t (kW)
P_t^{Grid}	Total power drawn from grid at time period t (kW)
$P_{i,e,t}^{\text{MCS,req}}$	Requested power from MCS operator for charging EV e at node i during time period t (kW)
$\text{SOE}_t^{\text{CESS}}, \text{SOE}_{m,t}^{\text{MCS}}, \text{SOE}_{e,t}^{\text{EV}}$	SOE value of CESS/MCS m/EV e in time period t (kWh)
$\mathfrak{I}^{\text{wait}}$	Total waiting time of EVs
$\mathfrak{I}_e^{\text{start}}$	Charging starting time of EV e
wt_e	Queue waiting time for EV e at charging station
$\mathbb{E}_{m,t}^{\text{way}}$	Total energy consumption for travel by MCS m in time period t (kWh)
$\mathbb{P}_{m,i,t}^{\text{dch,MCS}}$	Total power discharged by MCS m at node i in time period t (kW)
$\mathbb{P}_{i,t}^{\text{MCS,req}}$	Requested power from MCS operator for charging EVs at node i during time period t (kW)

E. Binary Variables

$x_{m,i,j,t}$	1 if MCS m travels using (i,j) route in time period t, else 0
$\mathcal{Y}_{i,e,t}, z_{i,e,t}$	1 if EV e connects to FCS/MCS at node i, in time period t, else 0
$\omega_{m,i,e,t}$	1 if EV e connects to MCS m at node i, in time period t, else 0
$\alpha_{e,t}^{\text{fx,start}}, \alpha_{e,t}^{\text{mcs,start}}$	1 if FCSs/MCSs start charging EV e in time period t, else 0
$\alpha_{e,t}^{\text{tot,start}}$	1 if charging of EV e starts in time period t, else 0
$\beta_{e,t}^{\text{fx,end}}, \beta_{e,t}^{\text{mcs,end}}$	1 if FCSs/MCSs finish charging EV e in time period t, else 0
$\delta_{m,i,t}^{\text{mcs,arr}}, \mu_{m,i,t}^{\text{mcs,dep}}, \kappa_{m,i,t}$	1 if MCS m arrives at/departs from/connects to node i, in time period t, else 0
ϱ_e	1 if MCSs reject to charge EV e, else 0
θ_t	Binary variable to prevent bidirectional power flow for CESS in time period t

1. Introduction

1.1 Motivation and Relevant Background

Energy consumption stands as the primary driver of greenhouse gas emissions, with heat and electricity generation accounting for 31.8% of these emissions [1]. The expansion and effective utilization of renewable energy sources (RESs) can significantly contribute to decreasing greenhouse gas emissions; however, the electricity generated by RESs is not always predictable, and this issue might result in challenges in maintaining the balance between energy supply and demand. Large-capacity electrical energy storage systems can be effectively used for minimizing the impact of uncertain behavior of RESs and increasing their utilization by storing the excess energy from RESs and injecting it especially during peak hours when prices are high.

Community energy storage systems (CESSs), consisting of shared battery storage units connected to low-voltage transformers that supply multiple homes or small businesses, can support RESs integration and enable flexible energy sharing among prosumers. CESSs are shared and utilized by the agents within a community. CESSs have been used in many studies as they are capable of providing a more economic option compared to individual battery energy storage systems by reducing system installation and maintenance costs [2]. A CESS sharing framework was proposed in [3] to reduce electricity costs and grid dependence of prosumers by considering both storage and power capacities. To reduce the curtailment of RES generation by storing the surplus energy in a CESS during the day for use during peak demand periods, the export limits for RESs were calculated in [4]. A power system consisting of a CESS and multiple RESs was considered in [5] with the objective of optimizing the operations and minimizing the total system cost. A coordination mechanism was proposed in [6] to enable collaboration between multiple community RES prosumers and a CESS, aiming to enhance local energy consumption and optimize renewable energy utilization while accounting for uncertainties in both supply and demand. The optimal operation of an energy community incorporating a CESS and shiftable loads was presented in [7] and costs, self-consumption and CO_2 emissions of the community were analyzed. While these studies demonstrate the potential of CESSs to reduce electricity costs and improve RES utilization, they do not address their integration for energy sharing within residential communities. This limitation reduces the effectiveness of CESSs in balancing load demand fluctuations and RES generation, restricting their ability to enhance energy self-sufficiency and optimize RES integration.

Recent research has focused on using CESSs for energy sharing in residential communities, optimizing the benefits of variable load demands and RES generation. The benefits of a CESS were evaluated for daily electricity cost and the self-consumption of photovoltaic (PV) energy for a residential community [8]. In [9], the flexibility constraints for an energy community and uncertain fluctuations in energy prices were considered and the level of the energy community self-sufficiency was examined with and without a CESS. An optimization strategy was proposed in [10] to reduce both the investment and operational expenses for CESS providers and prosumer operating costs, considering different energy pricing schemes and accounting for uncertainties in energy

consumption and PV generation. An energy cooperation approach between a CESS and several smart houses with rooftop PV systems and heating, cooling and air conditioning units was proposed in [11] for the purpose of minimizing energy cost and end-user discomfort. A similar approach was presented in [12] with the same objectives, by also considering the willingness of end users to participate in energy-sharing community. For a community consisting of a CESS and households with flexible loads and PV, a quota system-based energy management strategy was proposed in [13] to increase the fairness level among the prosumers while maximizing the CESS utilization.

In addition to the effective utilization of RESs, the transition to electric vehicles (EVs) also can mitigate greenhouse gas emissions significantly; however, none of the aforementioned studies considered the operation of CESSs with EVs. With this objective, a distribution substation including PVs, a 50 kWh CESS, and EVs was considered in [14] and it was shown that the impacts of EVs on grid, carbon emissions, and peak demand were reduced considerably with smart charging strategies. An energy community including household loads, PVs, shared EV chargers, and a 120 kWh CESS was considered in [15] with the objective of quantifying the benefits of CESS for an energy community and a distribution system operator, and minimizing the electricity and degradation costs for the community. However, these two studies did not examine the effect of distributed EV charging operations on the network and did not propose a CESS-based solution for reducing greenhouse gas emissions associated with EV charging.

Considering the economic, operational, and environmental benefits of CESSs mentioned in the given studies, it can be expected that similar benefits could be achieved for the communities including EVs if the charging and discharging operations of CESS are conducted by considering the EV arrival and departure time within the community. However, since CESS locations are fixed while EVs and EV charging stations are distributed over the community, the benefits of a single CESS might be limited due to the temporal and spatial mismatch between this unit and EV charging demands. To this end, the concept of mobile charging stations (MCSs) has emerged in the last years to effectively use energy storage systems for EV charging. MCSs eliminate the cost of purchasing or leasing land for fixed charging stations (FCSs), especially in city centers with limited suitable locations for building FCSs. Even in the presence of FCSs, MCSs can be used as a supplementary charging method to reduce the waiting times of EVs in FCSs, minimize time and energy spent for some EVs to reach FCSs, and increase the renewable energy utilization in EV charging, which results in a significant reduction in greenhouse gas emissions. The potential national benefits and business value of MCSs were analyzed in [16] and it was proven that MCSs can provide economic advantages by increasing the uptake of EVs and thereby reducing carbon emissions.

Several recent studies have been presented in the literature to evaluate the benefits of MCSs for EV charging. With the objective of reducing the charging costs, an optimization problem of scheduling and routing the MCSs was proposed in [17] by considering stochastic travel times of MCSs in the presence of spatio-temporal charging requests. A number of MCSs were used

in [18] to maximize the number of fully charged EVs, where an agent determines the route and schedule for each MCS. Instead of routing each EV, the MCS service strategy in [19] gathers multiple EVs in common charging places to mitigate the EV users' concerns about the lack of EV charging infrastructure. An MCS service optimization problem was divided into planning and operation in [20] where MCS dispatch was modeled as an EV routing problem at the operational level, and the number and locations of depots and MCS fleet size were determined at the planning level. For a multi time-scale EV charging service, an optimization approach combining the allocation, charging decision, and coordinated control of the MCSs at three different time scales (hours, minutes and seconds) was developed in [21]. In [22], to shorten the travel time of MCSs and prevent excessive MCSs from moving into the same areas simultaneously, a strategy that places idle MCSs in the areas with large potential charging demand was proposed. An assignment scheduling strategy of MCSs was proposed in [23], [24] and [25] where the assignments are scheduled to decrease the EV charging costs and increase the ratio of these EVs charged effectively. Several factors for providing MCS service to EVs such as distance to FCSs and distance to the nearest parking lot, arrival time at FCSs, arrival time at the nearest parking lot, and the average capacity of parking lots were considered in [26].

Despite their many benefits, it is anticipated that MCSs may not completely replace the role of FCSs in the short term due to their limited energy capacities. Therefore, a certain number of MCSs has been used with existing FCSs to meet the given charging demand of EVs. An algorithm was developed in [27] to determine the minimum number of MCSs and their optimal charging and discharging times and amounts to satisfy the given load demand of EVs, with the objective of reducing the operating cost of MCSs and an FCS. In [28], an optimization method was proposed to determine the optimal charging technology and location for EVs, considering EV travel trajectories. The study showed that MCSs might be the optimal charging method for many EV users as they reduce the EV user's overall charging cost and time. Besides, MCSs mitigate grid stress caused by EV charging at FCSs during peak hours. A dispatch algorithm for EVs was presented in [29] and the simulation results showed that when MCSs are used together with FCSs, the waiting time at FCSs reduces by 80%, and the peak demand on the network decreases by 8% for an EV penetration level of 25%. An energy management algorithm was introduced in [30] to investigate the benefits of MCSs in minimizing the number of EVs waiting for charging and improving grid operation. An economic operation of the MCSs was achieved by charging MCSs with RESs and the stress on grid was alleviated during high charging demand periods by charging some of the EVs through MCSs.

As outlined in the literature reviewed above, various studies have explored different charging infrastructure for EVs, including MCSs, CESSs, and FCSs. Each of these solutions offers distinct advantages, such as increased utilization of RES, reduced energy costs, and shorter charging times. However, none of these approaches independently provide all these benefits simultaneously due to their inherent limitations—FCSs have constrained capabilities, CESSs are not directly applicable for EV charging, and MCSs

lack the ability to support grid stability. By integrating and strategically coordinating these components, a more efficient and comprehensive charging infrastructure can be developed, optimizing benefits for all stakeholders.

1.2 Contribution

This study introduces a novel scheduling approach for optimizing the operation of multiple MCSs, FCSs, and a CESS, motivated by the potential of CESS to enhance renewable energy utilization, reduce greenhouse gas emissions, and enable load shifting, as well as the advantages of MCSs in providing fast and less greenhouse gas-intensive EV charging. Unlike existing models in the literature, the proposed framework explicitly integrates route selection, considering its impact on MCS travel times and energy consumption. Additionally, battery degradation costs for both CESS and MCSs are incorporated, addressing a factor frequently neglected in prior studies. The effectiveness of the proposed approach is analyzed from the perspective of key stakeholders, including distribution system operators, MCS and FCS operators, and EV users. The distinguishing features of the present study in comparison to existing research are tabulated in Table 1.

As seen from Table 1, most prior research focus on either FCSs or MCSs, whereas this study uniquely integrates both, in conjunction with a CESS, to enhance charging flexibility and accessibility. Furthermore, this study simultaneously optimizes multiple objectives, including minimizing carbon emissions, maximizing renewable energy utilization, facilitating load shifting, and minimizing EV charging times, considerations that are only partially addressed in prior research. While the previous studies do not account for key operational constraints, this study incorporates depot locations and battery degradation costs, ensuring a more realistic and economically viable optimization framework. By integrating these elements, the proposed framework presents a scalable and effective solution for EV charging infrastructure, effectively bridging critical research gaps.

The key contributions of this study are outlined as follows:

- A novel spatiotemporal scheduling algorithm is introduced to optimize EV charging in a given region, minimizing both carbon emissions and EV waiting times. This is the first study in the literature to address these objectives simultaneously.
- MCSs and a CESS are jointly utilized for the first time to address the limitations of FCSs, enabling optimal EV charging anytime and anywhere.
- Battery degradation costs for both MCSs and CESS, along with route constraints for MCSs, are considered, addressing the challenges mentioned in existing research.
- The impact of the proposed approach is comprehensively analyzed in terms of carbon emissions, EV waiting times at FCSs, and power demand from the grid. The evaluation leverages real-world EV charging profiles from the DERConnect Testbed at the University of California San Diego, and carbon emission data from the California Independent System Operator.

Table 1. Classification of the study in comparison to related studies in the literature.

Ref.	Objective/Benefit				CESS	Charging Station		Multiple Depot	Price Tariff	BDC
	Higher RES Utilization	Load Shifting	EVCM	EVC Time Minimization		FCS	MCS			
[3]	✓	×	×	×	✓	×	×	×	Dynamic	✓
[4]	✓	×	×	×	✓	×	×	×	ToU	×
[5]	✓	×	×	×	✓	×	×	×	Feed-in	×
[6]	✓	×	×	×	✓	×	×	×	Feed-in	×
[7]	✓	×	×	×	✓	×	×	×	Flat	✓
[8]	✓	×	×	×	✓	×	×	×	Volumetric	×
[9]	✓	×	×	×	✓	×	×	×	Dynamic	×
[10]	✓	×	×	×	✓	×	×	×	Feed-in	×
[11]	✓	×	×	×	✓	×	×	×	Dynamic	×
[12]	✓	×	×	×	✓	×	×	×	Feed-in	✓
[13]	✓	✓	×	×	✓	×	×	×	Dynamic	×
[14]	✓	✓	✓	×	✓	×	×	×	Dynamic	×
[15]	✓	×	✓	×	✓	×	×	×	Volumetric	✓
[16]	×	×	✓	×	×	×	✓	✓	Flat	×
[17]	×	×	✓	×	×	×	✓	×	-	×
[18]	×	×	✓	×	×	×	✓	×	-	×
[19]	×	×	✓	✓	×	×	✓	×	-	×
[20]	×	×	✓	✓	×	×	✓	✓	-	×
[21]	×	×	✓	✓	×	×	✓	✓	-	×
[22]	×	×	✓	✓	×	×	✓	×	-	×
[23]	×	×	✓	✓	×	×	✓	×	-	×
[24]	×	×	✓	✓	×	×	✓	×	-	×
[25]	×	×	✓	✓	×	×	✓	×	-	×
[26]	✓	✓	✓	✓	×	×	✓	×	Dynamic	×
[27]	✓	✓	✓	×	×	✓	✓	×	ToU	✓
[28]	×	✓	✓	✓	×	✓	✓	✓	ToU	×
[29]	×	✓	✓	✓	×	✓	✓	✓	ToU	✓
[30]	✓	✓	✓	✓	×	✓	✓	×	Dynamic	×
This Study	✓	✓	✓	✓	✓	✓	✓	✓	Dynamic	✓

Note: EVC: EV Charging, EVCM: EV Charging Management, BDC: Battery Degradation Cost

The remainder of the paper is structured as follows: Section 2 outlines the system architecture and formulates the problem for the proposed framework. Section 3 provides an analysis of the case studies and simulation results. Section 4 presents additional simulation analyses to validate the performance of the proposed algorithm across different scenarios, scales, and parameters, along with a comparative assessment against another optimization framework. An evaluation of the feasibility of MCSs is conducted in Section 5. Finally, Section 6 concludes the paper by summarizing the key findings.

2. Methodology

2.1 Framework Description

An EV charging framework is proposed to address the charging demands in a given area. This framework includes FCSs equipped with multiple charging units, MCSs supported by dedicated depots for recharging, and a CESS, as depicted in Fig. 1. The distribution system operator is assumed to own the FCSs and CESS, while the MCS operator manages the MCSs. EVs charge at FCSs based on real charging sessions, incorporating travel trajectories and time preferences derived from actual EV FCS data. At FCSs, EV users must wait for an available charging unit before they can begin charging, often leading to congestion and prolonged waiting times, especially during peak demand periods. To mitigate this issue, MCSs provide a more flexible and adaptive charging solution by adding additional chargers to a FCS site, thereby reducing waiting times and alleviating congestion at FCSs. When EV charging demand exceeds the capacity of FCSs, MCSs are dispatched to the FCSs based on their schedules and locations to supplement charging services. This deployment minimizes delays for EV users, and optimizes the overall utilization of the charging infrastructure.

The primary objective of the proposed framework is to reduce both carbon emissions and waiting times in EV charging operations. This is achieved by scheduling the charging of MCSs and CESS during periods of lower carbon emissions. Furthermore, the framework optimizes MCS routing based on EV user requests, minimizing MCS travel times, and reducing the corresponding energy consumption.

2.2 Mathematical Model of EV Charging Framework

The objective function for the proposed optimization problem and the mathematical models of the charging stations and CESS considered are described in the following subsections. The mathematical model is structured in two steps: the initial scheduling optimization and final validation phases in Step 1, and MCS routing optimization in Step 2. This framework facilitates the interaction between the distribution system operator and the MCS operator. A concise representation of these consecutive steps, summarizing the objective, constraints, and outputs for each, is presented in Fig. 2.

2.2.1 First Step of Mathematical Model

In the first optimization problem, the distribution system operator aims to minimize the carbon emissions caused by EV charging and the degradation of CESS and MCS batteries during charging and discharging operations.



Fig. 1. General schematic of the proposed system.

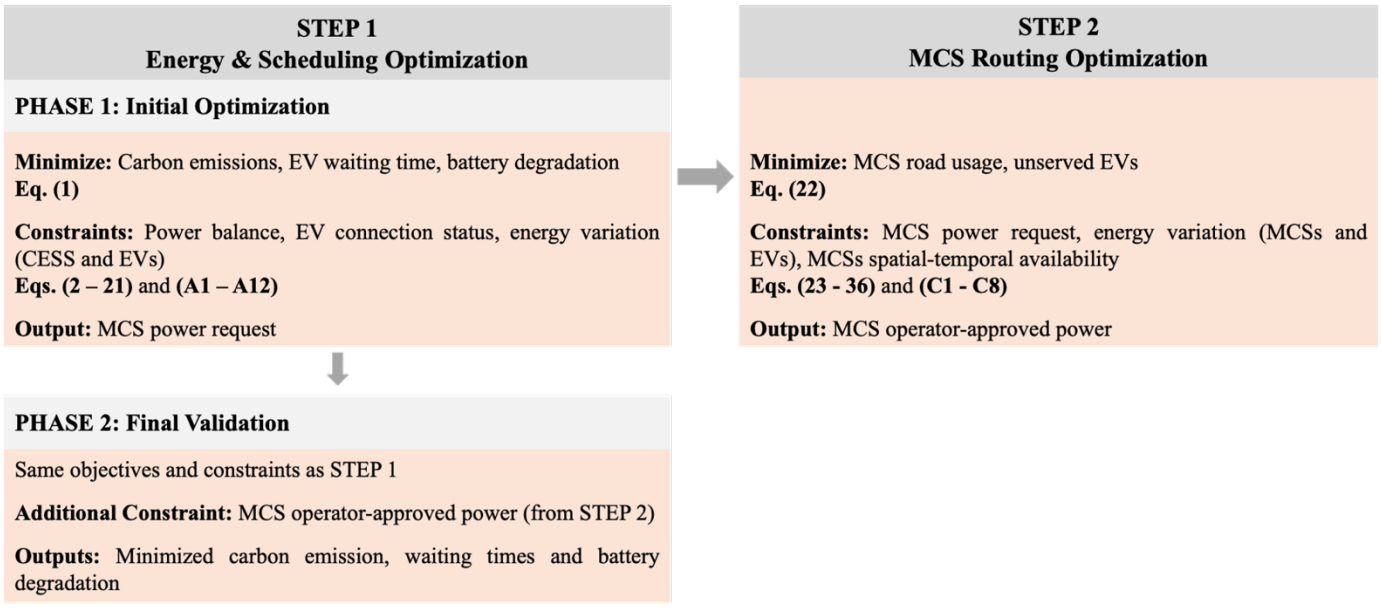


Fig. 2. Flowchart of the proposed two-step optimization framework.

Furthermore, the distribution system operator aims to minimize waiting times for EVs at FCSs to mitigate the clustering effect, where prolonged charger occupancy might overlap with residential or commercial peak loads, causing localized peak demand on the distribution system. To achieve these objectives, the operator utilizes energy from the grid and CESS, and requests additional energy from the MCS operator.

2.2.1.1 Objective Function

This study seeks to minimize carbon emissions from EV charging, waiting times at FCSs, and battery degradation in both MCSs and CESS. To achieve this, a cost is assigned to each objective, standardizing them in a common unit to facilitate optimization, enhance comparability, and improve interpretability. Accordingly, the proposed framework in Step 1 is designed to minimize the costs associated with carbon emissions, EV waiting times, and battery degradation, as outlined in (1).

$$min \sum_{t} \lambda_t^{\mathrm{CO2}} \cdot P_t^{\mathrm{Grid}} \cdot \Delta T + (\lambda^{\mathrm{CESSdeg}} \cdot P_t^{\mathrm{CESS,dch}} + \lambda^{\mathrm{MCSdeg}} \cdot P_t^{\mathrm{MCS,req}}) \cdot \Delta T + \lambda^{\mathrm{wait}} \cdot \Im^{\mathrm{wait}} \tag{1}$$

2.2.1.2 Power Exchange Constraints

The total power drawn from distribution network in time interval t comprises three components as shown in (2), where $P_t^{G\to\mathrm{FCS}}$ defines the amount of the power supplied to FCSs, $P_t^{G\to\mathrm{CESS}}$ is the power used to charge CESS and, $P_t^{G\to MCS}$ is the power for charging MCSs. The power demand of the EVs charged at the FCSs, $P_{i,e,t}^{\mathrm{ch,fx}}$, can be supplied by the grid or the CESS or both, as shown in (3). The total requested power from the MCSs at node i, $\mathbb{P}_{i,t}^{\mathrm{MCS,req}}$, is defined in (4) where $P_{i,e,t}^{\mathrm{MCS,req}}$ represents the power request of each EV e. Equation (5) ensures that the total charging power of MCSs, which is used to calculate the carbon emission contribution of MCSs in Step-1, equals the total requested power from MCSs. Equation (6) limits the charging power of MCSs in each time interval based on their charging rate. Constraint (7) restricts the permissible total discharging rate of MCSs at node i, while constraint (8) requires EV e to be connected to an MCS for energy transfer, adhering to the discharging rate limit, $\mathcal{R}^{\mathrm{dch,MCS}}$, of a single MCS.

$$P_t^{\mathrm{Grid}} = P_t^{G\to\mathrm{FCS}} + P_t^{G\to\mathrm{CESS}} + P_t^{G\to MCS}, \ \forall t \in T \tag{2}$$

$$P_t^{G\to\mathrm{FCS}} + P_t^{\mathrm{CESS}\to\mathrm{FCS}} = \sum_{i\in N',e\in E} P_{i,e,t}^{\mathrm{ch,fx}}, \forall t \in T \tag{3}$$

$$\mathbb{P}_{i,t}^{\mathrm{MCS,req}} = \sum_{e\in E} P_{i,e,t}^{\mathrm{MCS,req}}, \forall i \in N', \forall t \in T \tag{4}$$

$$\sum_{t\in T} P_t^{G\to MCS} = \sum_{i\in N',t\in T} (\mathbb{P}_{i,t}^{\mathrm{MCS,req}})/\Delta T \tag{5}$$

$$P_t^{G\to MCS} \le \mathcal{R}^{\mathrm{ch,MCS}}, \forall t \in T \tag{6}$$

$$\mathbb{P}_{i,t}^{\mathrm{MCS,req}} \leq \mathcal{R}^{\mathrm{MCS,tot}}, \forall i \in N', \forall t \in T \tag{7}$$

$$P_{i,e,t}^{\mathrm{MCS,req}} \leq \mathcal{R}^{\mathrm{dch,MCS}} \cdot z_{i,e,t}\ , z_{i,e,t} \in \{0,1\}, \forall e \in E, \forall i \in N', \forall t \in T \tag{8}$$

2.2.1.3 EV Charging Constraints

The state of energy (SOE) variation of EVs is defined as the SOE of EV e upon arrival at node i, where an FCS is located, plus the energy charged to EV e in time interval t using one of the available charging methods—either an FCS or an MCS—as expressed in (9). The battery SOE of EVs, $\mathrm{SOE}_{e,t}^{\mathrm{EV}}$, is limited by (10) between initial and requested SOE levels. Constraints (11) and (12) ensure that the SOE level of EV e is greater than or equal to the requested energy level, $\mathrm{SOE}_{e}^{\mathrm{req}}$, when charging is completed. Connection status constraints of the EVs are given in Appendix A.

$$\mathrm{SOE}_{e,t}^{\mathrm{EV}} = \mathrm{SOE}_{e,t-1}^{\mathrm{EV}} + \sum_{i \in N'} (P_{i,e,t}^{\mathrm{ch,fx}} \cdot \eta^{\mathrm{fx}} + P_{i,e,t}^{\mathrm{MCS,req}} \cdot \eta^{\mathrm{mcs}}) \cdot \Delta T, \forall e \in E, \text{if } t \neq t^0 \tag{9}$$

$$\mathrm{SOE}_{e}^{\mathrm{EV,ini}} \leq \mathrm{SOE}_{e,t}^{\mathrm{EV}} \leq \mathrm{SOE}_{e}^{\mathrm{req}}, \forall e \in E, \forall\, t \in T \tag{10}$$

$$\mathrm{SOE}_{e,t}^{\mathrm{EV}} \geq \mathrm{SOE}_{e}^{\mathrm{req}} \cdot \beta_{e,t}^{\mathrm{fx,end}}\ , \beta_{e,t}^{\mathrm{fx,end}} \in \{0,1\}, \forall e \in E, \forall\, t \in T \tag{11}$$

$$\mathrm{SOE}_{e,t}^{\mathrm{EV}} \geq \mathrm{SOE}_{e}^{\mathrm{req}} \cdot \beta_{e,t}^{\mathrm{mcs,end}}, \beta_{e,t}^{\mathrm{mcs,end}} \in \{0,1\}, \forall e \in E, \forall\, t \in T \tag{12}$$

2.2.1.4 FCS Operation Constraints

Equation (13) imposes a limit on the charging power of EV e, ensuring it does not exceed the charger's power capacity. The binary variable $y_{i,e,t}$ ensures that EV e is connected to a fixed charger at node i within time interval t. Constraint (14) limits the charging power of FCS to the total permissible power at node i. As indicated in (15), the number of connected EVs cannot exceed the number of chargers at node i.

$$P_{i,e,t}^{\mathrm{ch,fx}} \leq \mathcal{R}_{i}^{\mathrm{fx}} \cdot y_{i,e,t}\ , y_{i,e,t} \in \{0,1\}\ , \forall e \in E, \forall i \in N', \forall t \in T \tag{13}$$

$$\sum_{e \in E} P_{i,e,t}^{\mathrm{ch,fx}} \leq \mathcal{R}_{i}^{\mathrm{fx}} \cdot C_{i}^{\mathrm{fx}}\ , \forall i \in N', \forall t \in T \tag{14}$$

$$\sum_{e \in E} y_{i,e,t} \leq C_{i}^{\mathrm{fx}}\ , y_{i,e,t} \in \{0,1\}\ , \forall i \in N', \forall t \in T \tag{15}$$

2.2.1.5 CESS Operation Constraints

The charging power of the CESS is equal to the power drawn from the grid for each time interval t as per (16). The discharging power of the CESS is equal to the power transferred to FCSs as per (17). Besides, the charging and discharging power of the CESS are limited by the charging/discharging rating $\mathcal{R}^{\mathrm{CESS}}$, while the binary variable θ_t prevents simultaneous charging and discharging of the CESS. The SOE variation of CESS is depicted in (18) based on the charging and discharging powers, while the SOE at any

given time period is constrained within the minimum and maximum values in (19). Constraints (20) and (21) ensure that the SOE of the CESS at the start and end of the day remains equal to the initial SOE. Lastly, the battery degradation rate calculation for CESS and MCSs is provided in Appendix B.

$$P_t^{\mathrm{ch,CESS}} = P_t^{G\to\mathrm{CESS}} \le \mathcal{R}^{\mathrm{CESS}} \cdot \theta_t \ , \theta_t \in \{0,1\} \, , \forall t \in T \tag{16}$$

$$P_t^{\mathrm{dch,CESS}} = P_t^{\mathrm{CESS}\to\mathrm{FCS}} \le \mathcal{R}^{\mathrm{CESS}} \cdot (1-\theta_t) \ , \theta_t \in \{0,1\} \, , \forall t \in T \tag{17}$$

$$\mathrm{SOE}_t^{\mathrm{CESS}} = \mathrm{SOE}_{t-1}^{\mathrm{CESS}} + (P_t^{\mathrm{ch,CESS}} \cdot \Delta T \cdot \eta^{\mathrm{ch}}) - (P_t^{\mathrm{dch,CESS}} \cdot \Delta T / \eta^{\mathrm{ch}}) \, , \mathrm{if}\, t \neq t^0 \tag{18}$$

$$\mathrm{SOE}^{\mathrm{CESS,min}} \le \mathrm{SOE}_t^{\mathrm{CESS}} \le \mathrm{SOE}^{\mathrm{CESS,max}} , \forall\, t \in T \tag{19}$$

$$\mathrm{SOE}_t^{\mathrm{CESS}} = \mathrm{SOE}^{\mathrm{CESS,ini}} , \mathrm{if}\, t = t^0 \tag{20}$$

$$\mathrm{SOE}_t^{\mathrm{CESS}} = \mathrm{SOE}^{\mathrm{CESS,ini}} , \mathrm{if}\, t = t^{\mathrm{end}} \tag{21}$$

2.2.2 Second Step of the Mathematical Model

The second optimization problem takes the perspective of the MCS operator, focusing on minimizing the energy spent by the MCSs while traveling and ensuring the power requested by the power system operator is delivered to the EVs.

2.2.2.1 Objective Function

The proposed framework in Step 2 aims to minimize the energy consumption of MCSs during transit, $\mathbb{E}_{m,t}^{\mathrm{way}}$, as well as the number of unserved EVs, λ^{miss}, as indicated in (22).

$$\min \sum_{m,t} \mathbb{E}_{m,t}^{\mathrm{way}} + \lambda^{\mathrm{miss}} \cdot \ \varrho_e \ , \varrho_e \in \{0,1\} \tag{22}$$

2.2.2.2 MCS Power and Energy Constraints

Constraints (23) to (30) define the framework for the charging and discharging processes of MCSs. In (23), MCSs charging power, $P_{m,i,t}^{\mathrm{ch,MCS}}$, is constrained by the charging ratings of the depot chargers, and MCS charging is permitted only during hours with minimum carbon emissions ($t \in T'$), as defined in Step-1. The binary variable $\kappa_{m,i,t}$ requires that MCS m is connected to node i for self-charging. Equation (24) prevents MCSs from charging outside the depot locations. The total discharging power of MCSs, $\mathbb{P}_{m,i,t}^{\mathrm{dch,MCS}}$, is defined in (25), while in (26), it is restricted by the total discharging rate of all chargers on the MCS. Since MCSs only serve the EVs identified in Step 1, the total MCS power is less than or equal to the power requested by the EVs as indicated in (27). Equation (28) specifies whether the EVs assigned to MCSs are accepted and charged or rejected, with rejected EVs being represented by the binary variable ϱ_e for penalization. Constraint (29) requires that EV e be connected to an MCS for power transfer ensured by the binary variable $\omega_{m,i,e,t}$. Constraint (30) prohibits the discharging of MCSs at depot locations.

The SOE constraints are outlined in (31) through (36). In (31), the SOE of MCSs, $\mathrm{SOE}_{m,t}^{\mathrm{MCS}}$, is determined by the charging and discharging rate, as well as the energy consumption for travel by MCS m in time period t. Equation (32) imposes limits on the SOE of MCSs to prevent both overcharging and deep discharging. Constraints (33) and (34) ensure that the SOE of each MCS at the end of the day is equal to the SOE at the beginning of the day. In (35), the energy spent in transit by MCS m in time period t is given. Constraint (36) formulates the energy consumed by MCS m while traveling between nodes as a function of distance and energy consumption per unit distance for MCSs. The binary variable $x_{m,i,j,t}$ is set to 1 if MCS m travels along route (i, j) during time period t, and 0 otherwise. MCS operation constraints are provided in Appendix C.

$$P_{m,i,t}^{\mathrm{ch,MCS}} \le \mathcal{R}^{\mathrm{ch,MCS}} \cdot \kappa_{m,i,t} \ , \kappa_{m,i,t} \in \{0,1\}, \forall m \in M, \forall i \in N^{1,2}, \forall t \in T' \tag{23}$$

$$P_{m,i,t}^{\mathrm{ch,MCS}} = 0 \ , \forall m \in M, \forall i \in N', \forall t \in T \tag{24}$$

$$\mathbb{P}_{m,i,t}^{\mathrm{dch,MCS}} = \sum_{e \in E} P_{m,i,e,t}^{\mathrm{dch,MCS}} \ , \forall m \in M, \forall i \in N', \forall t \in T \tag{25}$$

$$\mathbb{P}_{m,i,t}^{\mathrm{dch,MCS}} \le \mathcal{R}^{\mathrm{dch,MCS}} \cdot C_{m}^{\mathrm{MCS}} \cdot \kappa_{m,i,t} \ , \kappa_{m,i,t} \in \{0,1\}, \forall m \in M, \forall i \in N', \forall t \in T \tag{26}$$

$$\sum_{m \in M} P_{m,i,e,t}^{\mathrm{dch,MCS}} \le \ P_{i,e,t}^{\mathrm{MCS,req}} \tag{27}$$

$$\sum_{m \in M, i \in N', t \in T} P_{m,i,e,t}^{\mathrm{dch,MCS}} \cdot \Delta T \cdot \eta^{\mathrm{mcs}} \ \ge \mathrm{SOE}_{e}^{\mathrm{req}} \cdot (1 - \varrho_e) \ , \varrho_e \in \{0,1\} \ , \forall e \in E \tag{28}$$

$$P_{m,i,e,t}^{\mathrm{dch,MCS}} \le \mathcal{R}^{\mathrm{dch,MCS}} \cdot \omega_{m,i,e,t} \ , \omega_{m,i,e,t} \in \{0,1\} \ , \forall m \in M, \forall e \in E, \forall i \in N', \forall t \in T \tag{29}$$

$$\mathbb{P}_{m,i,t}^{\mathrm{dch,MCS}} = 0 \ , \forall m \in M, \forall i \in N^{1,2}, \forall t \in T \tag{30}$$

$$\mathrm{SOE}_{m,t}^{\mathrm{MCS}} = \mathrm{SOE}_{m,t-1}^{\mathrm{MCS}} + \sum_{i \in N} (P_{m,i,t}^{\mathrm{ch,MCS}} \cdot \eta^{\mathrm{mcs}} - \mathbb{P}_{m,i,t}^{\mathrm{dch,MCS}}) \cdot \Delta T \ - \ \mathbb{E}_{m,t}^{\mathrm{way}} , \forall m \in M, \mathrm{if}\, t \ne t^{0} \tag{31}$$

$$\mathrm{SOE}^{\mathrm{MCS,min}} \le \mathrm{SOE}_{m,t}^{\mathrm{MCS}} \le \mathrm{SOE}^{\mathrm{MCS,max}}, \forall m \in M, \forall\, t \in T \tag{32}$$

$$\mathrm{SOE}_{m,t}^{\mathrm{MCS}} = \mathrm{SOE}^{\mathrm{MCS,ini}}, \mathrm{if}\, t = \ t^{0} \tag{33}$$

$$\mathrm{SOE}_{m,t}^{\mathrm{MCS}} = \mathrm{SOE}^{\mathrm{MCS,ini}}, \mathrm{if}\, t = \ t^{\mathrm{end}} \tag{34}$$

$$\mathbb{E}_{m,t}^{\mathrm{way}} = \sum_{i \in N, j \in N} E_{m,i,j,t}^{\mathrm{way}} \ , \forall m \in M, \forall (i,j) \in R, \forall t \in T \tag{35}$$

$$E_{m,i,j,t}^{\mathrm{way}} = \sigma^{\mathrm{way}} \cdot \mathcal{D}_{i,j} \cdot x_{m,i,j,t} \ , x_{m,i,j,t} \in \{0,1\} \ , \forall m \in M, \forall (i,j) \in R, \forall t \in T \tag{36}$$

Finally, Phase 2 of Step 1 validates the power flows in the system, based on the interactions between the distribution system operator and MCS operator. In this phase, Phase 1 is re-evaluated based on the results from Step 2. If the EV charging request

submitted to the MCS operator in Phase 1 of Step 1 is fully accepted in Step 2, no further action is needed. However, if the MCS operator only partially meets the charging request of the power system operator, Phase 2 of Step 1 takes the accepted portion as a parameter and re-solves Phase 1.

This study considers predetermined charging demands based on real-world data, including arrival time and the initial and requested SOE levels of the EVs. Since reservation-based systems are commonly used in MCSs and FCSs, this assumption is realistic. While the proposed algorithm can be adapted for dynamic inputs, our previous research [31-32] suggests that this would have minimal impact on the results. However, if required, the methodology can be modified to function as a real-time algorithm as in [33]. For this purpose, the problem should be solved at each episode ($p \in P$), with all variables stored for the next episode. From this perspective, the charging demand parameters— $\mathrm{SOE}_e^{\mathrm{EV,ini}}$, $\mathrm{SOE}_e^{\mathrm{req}}$, and $\mathrm{arr}_{e,t}^{\mathrm{EV}}$ —should be adapted at each episode by introducing an additional dimension. Consequently, in the first episode, the optimization problem will be solved using charging reservation data only, without knowledge of real charging demands. In subsequent episodes, the optimal solutions will dynamically adjust based on the charging demand history.

3. Case Studies and Results

3.1 Input Data

To evaluate the effectiveness of the proposed approach, real data from the DERConnect Microgrid Testbed located within the University of California San Diego Campus, which is comprised of solar PV generators, battery energy storage systems, level 2 and DC fast chargers EV charging stations, and energy efficient buildings with flexible loads, are used. The proposed Mixed-Integer Linear Programming (MILP) optimization problem is solved using the General Algebraic Modeling System (GAMS) v.25.1.3, in conjunction with the CPLEX commercial solver, with a 15-minute time resolution. The locations of the CESS and FCSs as well as the recharging locations for the MCSs (marked with red triangles) are shown in Fig. 3.

We used data from Tuesday, April 30, 2024, the latest available day in a dataset of FCS at University of California San Diego. This dataset provides the battery capacities, actual energy charged, and arrival-departure times of 126 EVs over 49 different models/brands as presented in Fig. 4. EV arrival and departure times are assumed to be known a priori, consistent with common practice in the literature [14, 16-19, 23, 25-30, 41], as accounting for unknown times would not significantly enhance our analysis [31-32]. To meet the daily charging demand of these EVs, 4 identical MCSs, along with 10 Level 2 and 3 DC fast chargers FCSs plazas located at different locations on the campus, were deployed. The Level 2 FCSs are assumed to be equipped with four chargers each, the DC fast chargers FCSs with three chargers each, and the MCSs with three plugs each. In addition, 600 kWh of a 5,000 kWh CESS was allocated for EV charging to shift grid energy consumption to periods of lower carbon emissions. The technical specifications of the CESS and MCSs are provided in Table 2.



Fig. 3. The location of the CESS, FCSs and MCS charging depots at the University of California San Diego Campus.

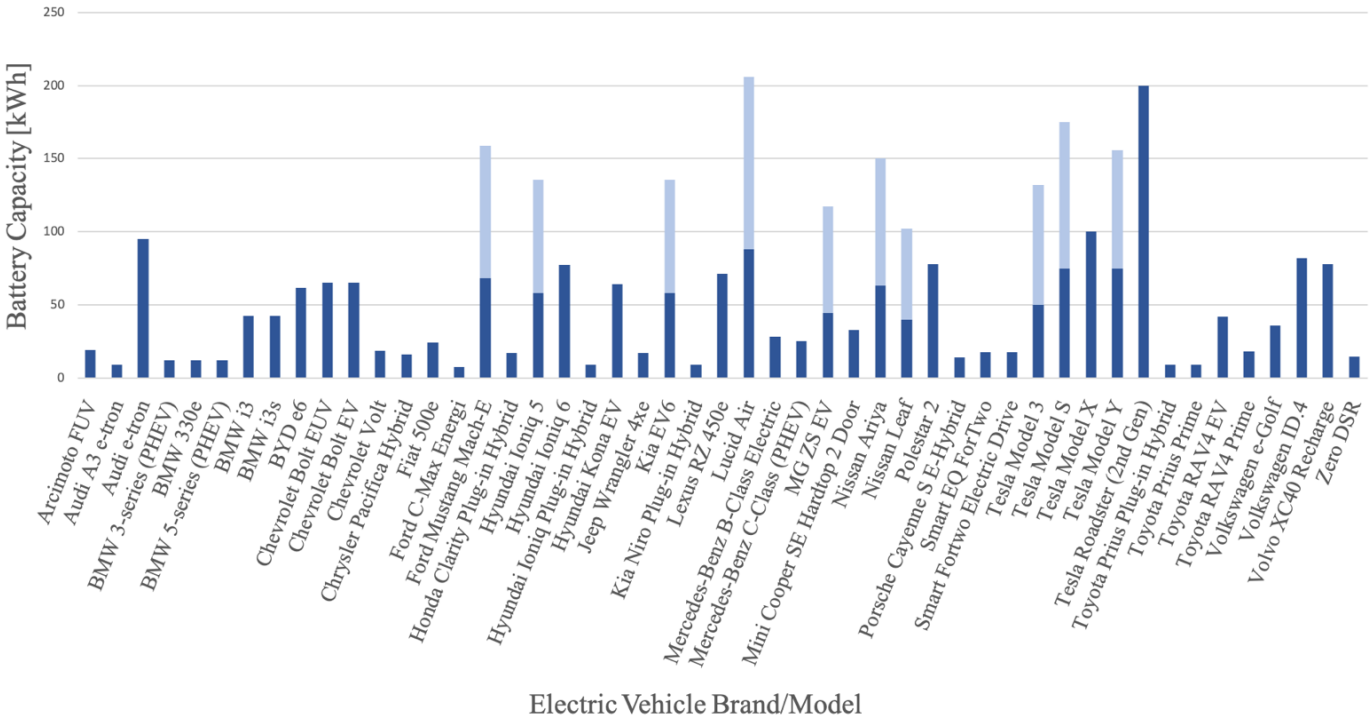


Fig. 4. Battery capacities of EVs considered in the study. Some models have multiple variants featuring different battery capacities, with the range of capacities depicted by a light blue bar.

The initial SOE level of the CESS and MCSs was set to 50% of their battery capacity. The SOE levels were constrained within a range of 10% to 90% of the total battery capacity. The 10% lower limit mitigates capacity loss, voltage instability, and premature degradation, while the 90% upper limit prevents overheating, chemical deterioration and capacity reduction. These thresholds align with EV manufacturer guidelines [34-35] and prevailing research practices [36-38]. The unit price of lithium-ion batteries is assumed to be $100/kWh, with a cycle life of 2,000 cycles at an 80% DoD and a salvage value of 60% of the capital cost. The maximum charging/discharging rates for CESS and MCS are 300 kW and 125 kW, respectively. Additionally, an activation energy of 40,000 J/mol, a pre-exponential factor of 2.8×10^6, and temperature of 45°C are considered. Based on these assumptions, the battery degradation costs for CESS, $\lambda^{\mathrm{CESSdeg}}$, and MCS, $\lambda^{\mathrm{MCSdeg}}$, are calculated to be $0.00394/kWh and $0.00350/kWh, respectively. Carbon emission and locational marginal electricity price data from California Independent System Operator on April 30, 2024 are shown in Fig. 5.

Table 2. Technical specifications of CESS and MCSs [39].

	SOE [kWh]	Charging/Discharging Efficiency [%]	Road Energy Consumption [kWh/km]	Max. Charging/Discharging rate [kW]
CESS	600	0.95	-	300
MCS	250	0.95	0.304	125

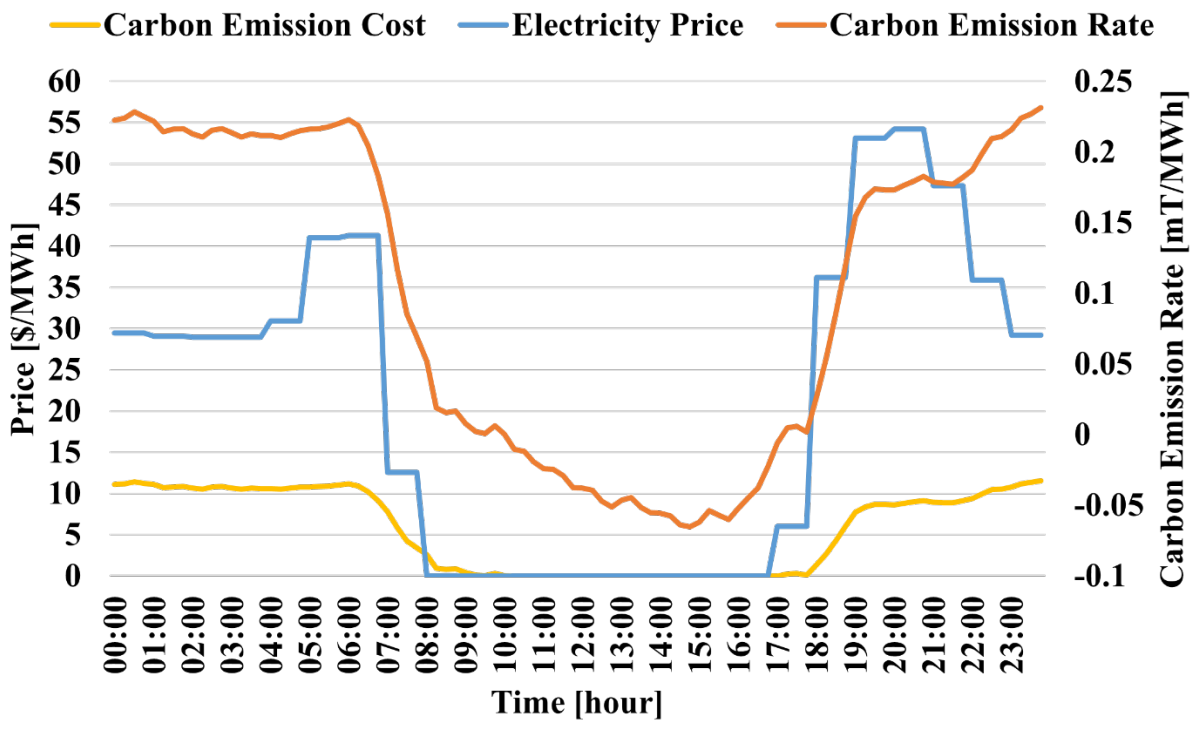


Fig. 5. Electricity price, carbon emission price and rate for the considered day [40].

Figure 5 also presents the carbon emission cost throughout the day, calculated based on the social cost of carbon, which is estimated by the U.S. government at $50 per metric ton (m.T.) [41]. It can be seen from Fig. 5 that the carbon emission cost, carbon emission rate, and electricity price are significantly reduced during noon and afternoon hours due to the increased power production from a large number of PVs in California and its vicinity at those times.

3.2 Simulation and Results

To assess the benefits, the proposed framework is evaluated against two cases, which are Base Case and Case 1:

- Base Case: 13 FCSs are used for EV charging, and the CESS is not integrated into the system.
- Case 1: 13 FCSs are used for EV charging, with the CESS integrated into the system.
- Case 2: Both 13 FCSs and 4 MCSs are employed for EV charging, and the CESS is integrated into the system.

In the Base Case, the charging demand of all EVs is entirely met by the FCSs, which rely on grid power throughout the day. It can be seen from Fig. 6 that in Case 1, where the CESS is employed, and in Case 2, where both the CESS and MCSs are utilized, the EV charging demand during early morning, evening, and nighttime is fully covered by the CESS and MCSs. During other periods, when the carbon emission cost is zero or near zero, the grid power is used to meet the charging demand in all cases. The power contributions from the CESS in Case 1 and Case 2 are depicted in Fig. 7. In Case 2, 47.6% of the EV charging demand is met by the MCSs rather than the CESS, resulting in reduced CESS power utilization. Figure 8 shows the charging and discharging power of the CESS for Case 1 and Case 2. When Figs. 5 and 8 are analyzed together, it is evident that the CESS charges during periods of low carbon emissions and discharges during periods of high-emissions to minimize the carbon footprint associated with EV charging. As a result of these charging and discharging cycles, the variation in the SOE of the CESS along with its upper and lower bounds are depicted in Fig. 9. The charging profiles of the CESS in both Case 1 and Case 2 exhibit a high degree of similarity. In other words, the CESS can be charged over a wide time range (10:15–17:00), when carbon emissions are zero, and discharged during high-emission periods to reduce the grid power consumption.

The charging and discharging powers of the MCSs in Case 2 as well as their routes are determined based on the results of Phase 1 of Step 1. In this phase, $P_{i,e,t}^{\mathrm{MCS,req}}$ is calculated considering the carbon emission cost and the waiting time of EVs. The charging/discharging powers and routes of the MCSs are then optimized in Step 2. Figure 10 shows the SOE variation for each MCS and the total charging/discharging power of the MCSs. The figure shows that MCS charging is constrained to minimum emission periods, as per constraint (23), while MCS discharging varies depending on EV charging requests. The variation in SOE among the MCSs is attributed to differences in EV charging demands with respect to location, time and, requested energy. Lastly, to demonstrate how FCSs, MCSs, and CESS work together to satisfy the EV charging demands, Fig. 11 illustrates the individual power contributions from each system in Case 2. The CESS and MCSs supplied 24.7% of the EV charging demand in Case 2, leading to reduced CO_2 emissions and eliminate waiting times.

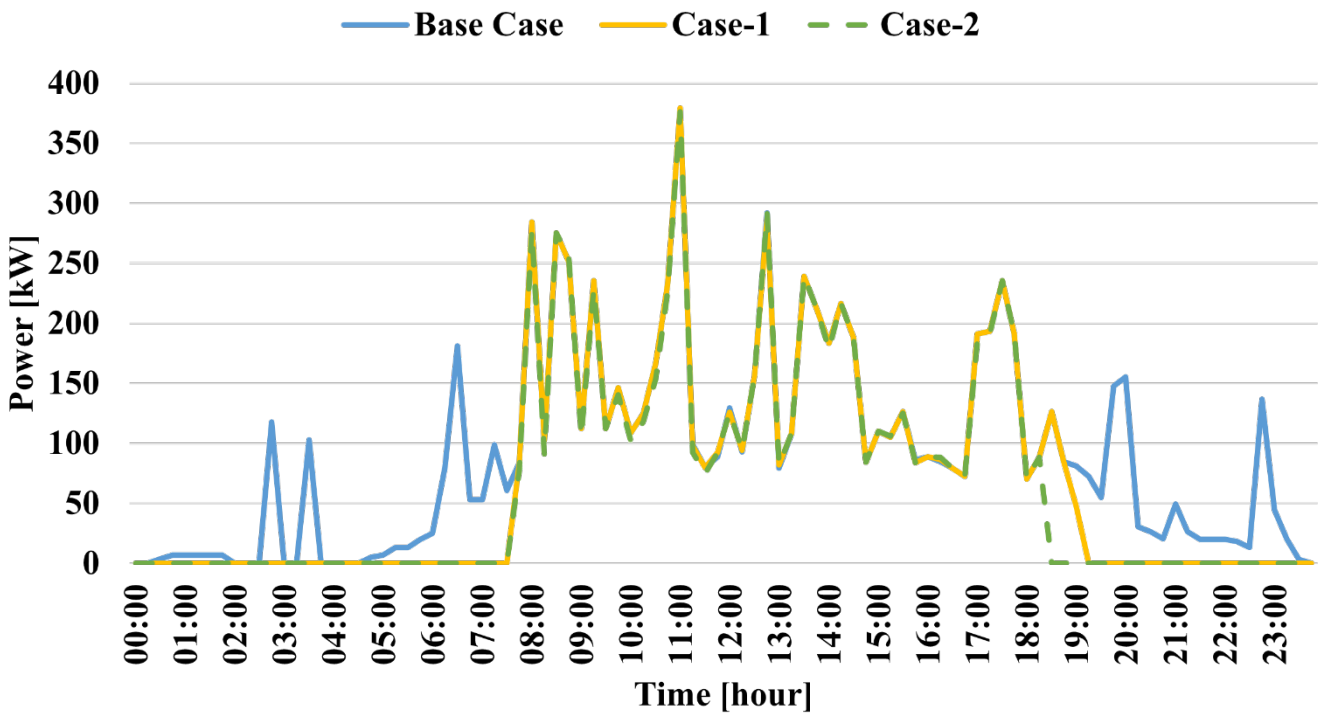


Fig. 6. FCS EV charging power drawn from the grid for all cases.

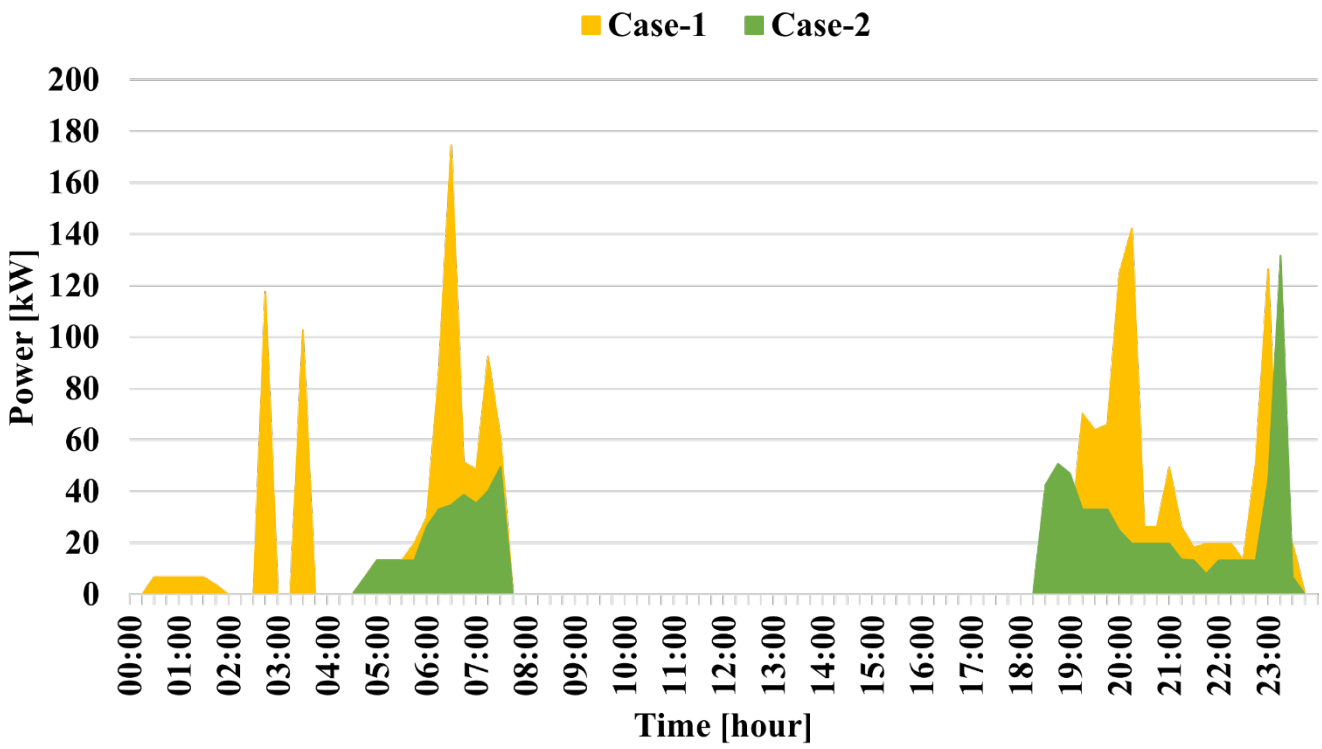


Fig. 7. FCS EV charging power drawn from the CESS for Cases 1 and 2.

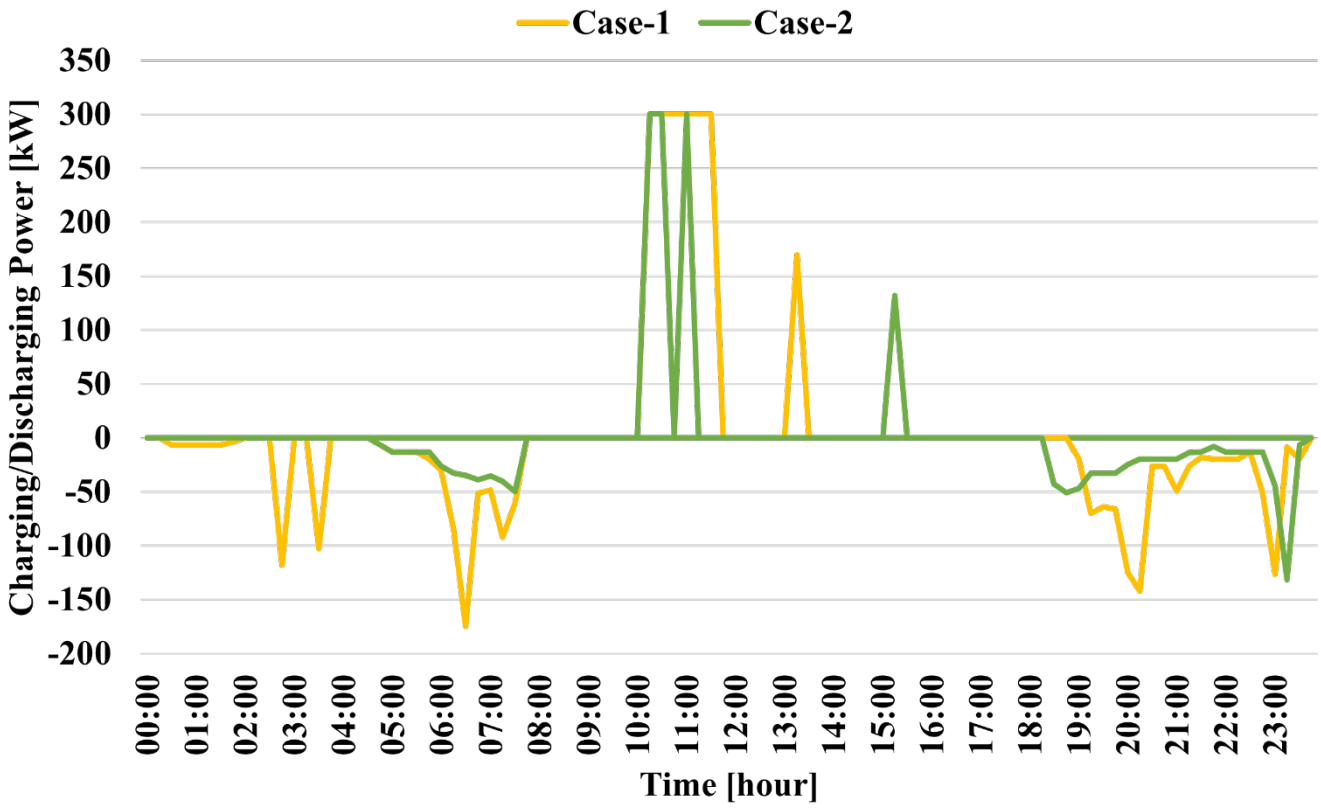


Fig. 8. CESS charging (positive) and discharging (negative) power for Cases 1 and 2.

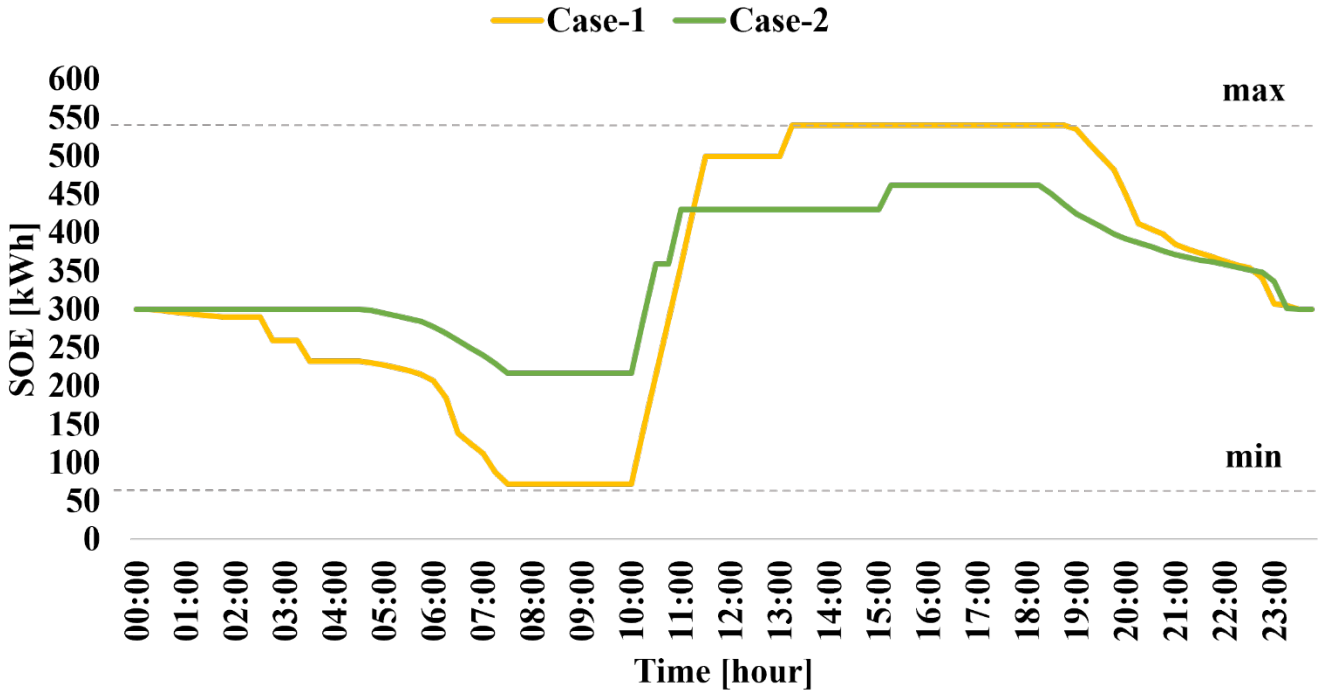


Fig. 9. CESS SOE variation for Cases 1 and 2.

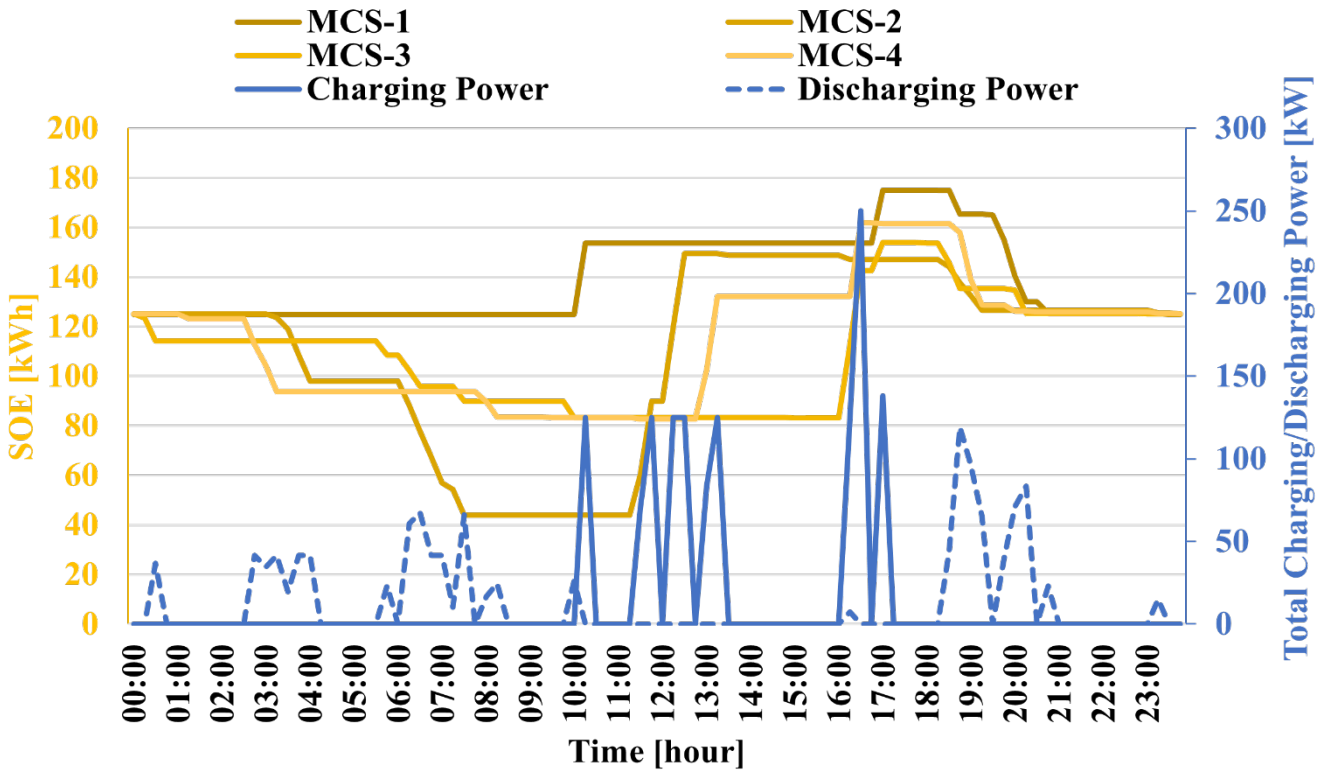


Fig. 10. MCS power and SOE variations for Case 2. The charging and discharging power is the sum of all MCSs.

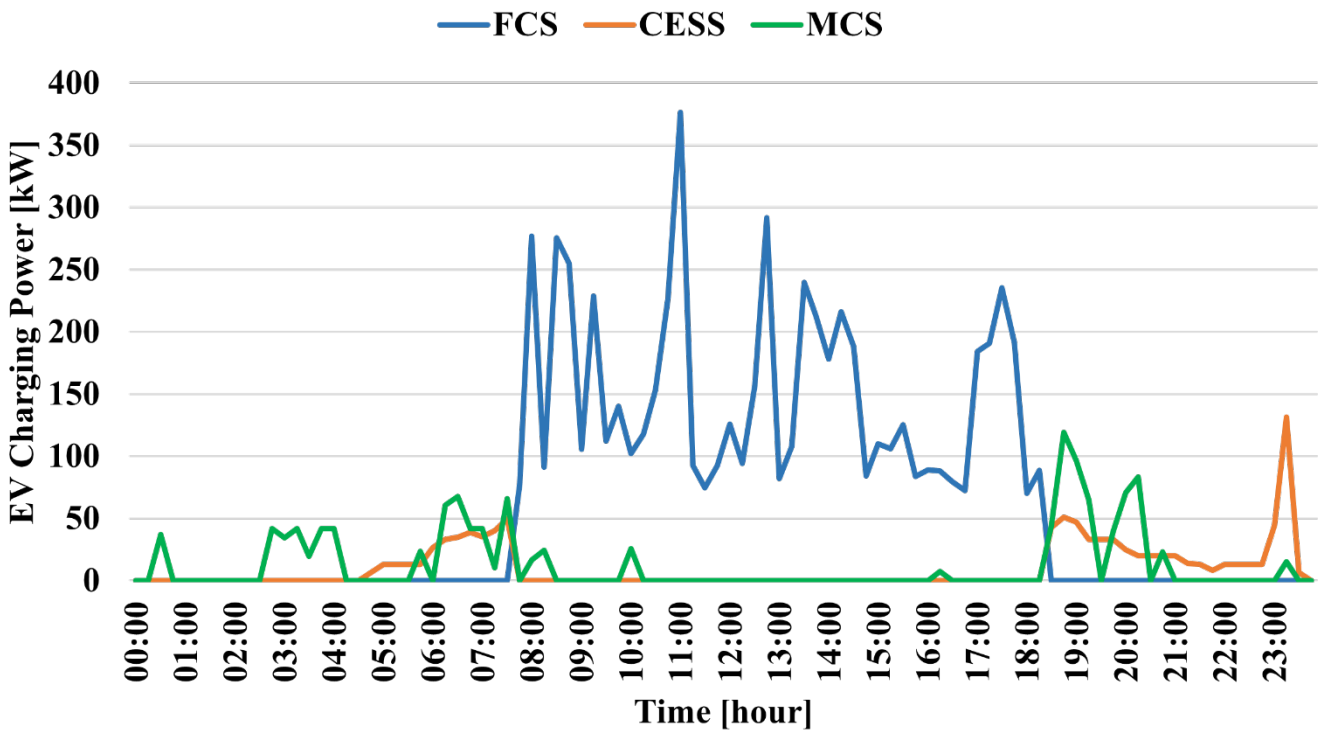


Fig. 11. EV charging power drawn from the FCS, CESS and MCSs for Case 2.

The assignment of EVs to MCSs and their corresponding FCSs is determined during the optimization process in Phase 1 of Step 1, taking into account the congestion levels at the FCSs, as outlined in Table 3. The FCS locations accessed by the MCSs and their routes in Case 2 are illustrated in Fig. 12, with each route shown in a distinct color across four subfigures. For clarity, a limited area of the University of California San Diego map is displayed in Fig. 12. To meet all EV charging requests and follow the most efficient routes, MCSs may need to recharge multiple times at depot locations.

The total cost and its components, which are waiting time cost, battery degradation cost, and carbon emission cost, are illustrated in Fig. 13. In the Base Case, without the integration of MCS and CESS, EV charging leads to high carbon emissions and longer waiting times, which raises the total cost. When the CESS is introduced into the system, carbon emission costs decrease by 82%; however, a battery degradation cost of $1.8 is incurred as a trade-off. In Case 2, where both the CESS and MCS are implemented, carbon emission costs decrease by 44.4% compared to Case 1, and waiting times at the charging stations are reduced to zero. Consequently, most of the total cost for Case 2 consists of battery degradation. Table 4 presents a comparison of carbon emissions, EV charging time, peak electricity demand, and total electricity cost across all three cases. The first column clearly demonstrates the effectiveness of energy storage technologies in reducing carbon emissions, as they are primarily charged with emission-free energy and discharged to supply the required energy for EV charging during high-emission periods.

Table 3. Assignment of EVs to FCSs and MCSs for Case 2.

Charging Stations	**Charger Type**	**Total EV Number**	**EVs assigned to FCSs**	**EVs assigned to MCSs**
P017 (Birch Aquarium)	Level 2	5	5	0
Services Complex		3	3	0
P206 (Faculty Club)		3	3	0
Gilman PS		20	12	8
P014 (Keck)		2	2	0
Mesa Nueva PS		10	9	1
Mesa Canyon PS		17	10	7
P610		12	10	2
P703 (ECUP)		15	13	2
Torrey Pines Court		3	3	0
Athena PS	DC fast chargers	22	16	6
Mesa Canyon PS		5	3	2
South PS		9	8	1

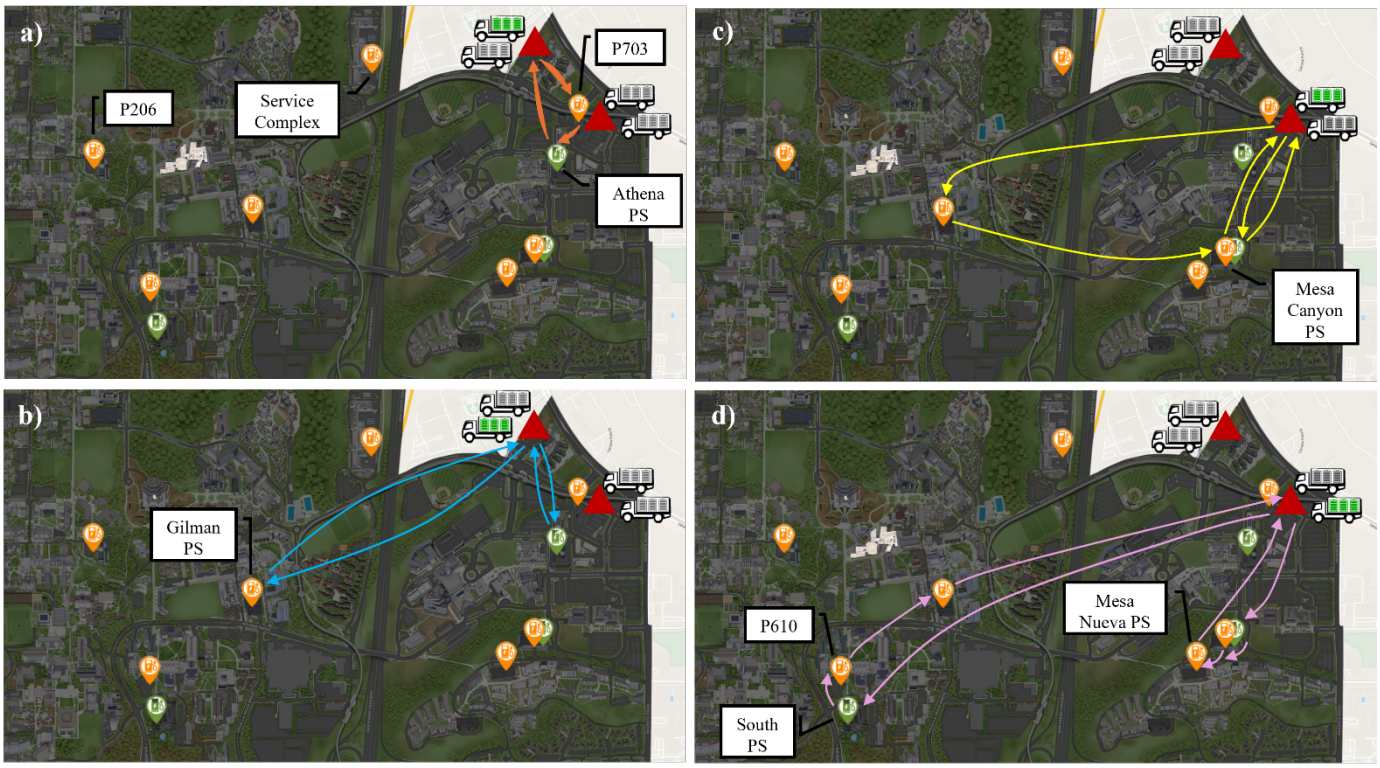


Fig. 12. The route of a) MCS-1, b) MCS-2, c) MCS-3, d) MCS-4.

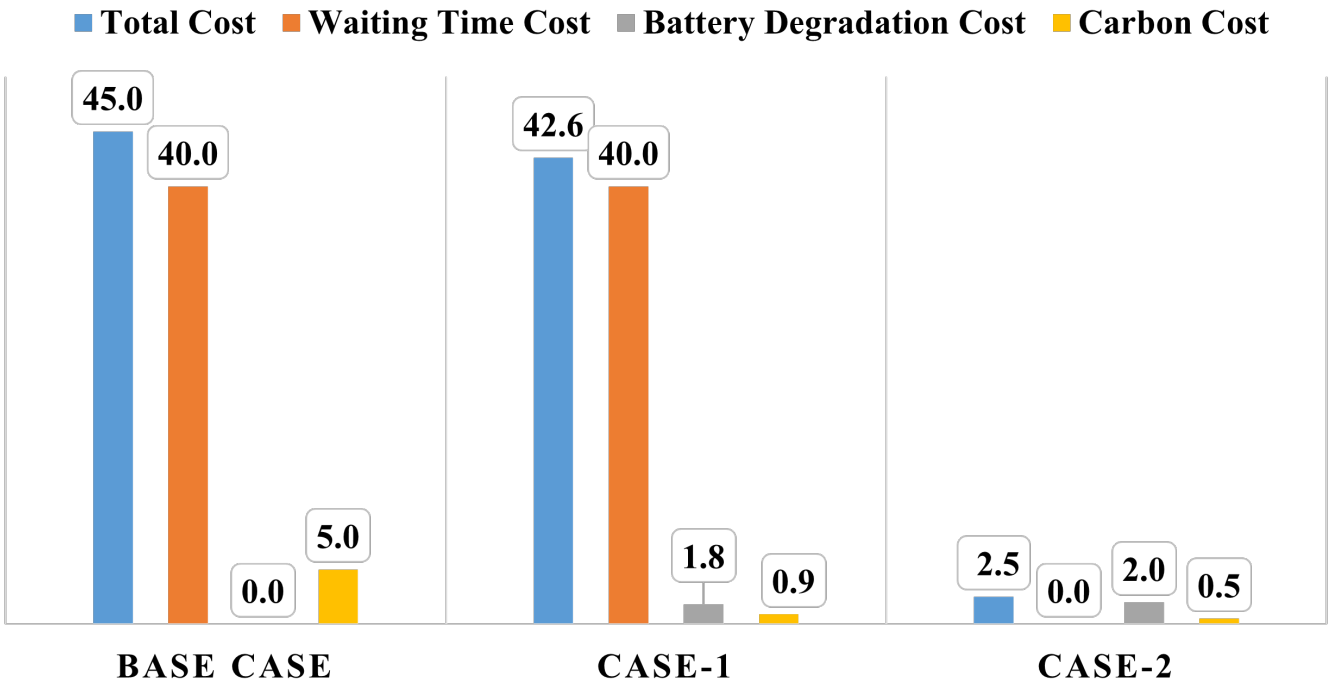


Fig. 13. Comparison of the costs for all cases.

Table 4. Comparison of carbon emissions, waiting times, peak electricity demand, and electricity costs for all cases.

	Carbon emission [kgCO_2/day]	EV waiting time [mins/day]	Peak electricity demand [kWh/day]	Total electricity cost [$/day]
FCSs	100.3	150.0	176.0	22.9
Case 1	17.7	150.0	11.9	5.5
Case 2	10.4	0.0	0.0	3.1

Furthermore, Table 4 highlights that MCSs can alleviate the need for EVs to wait at FCSs for charging services. The use of energy from storage systems results in battery degradation costs, which prevents the algorithm from achieving zero carbon emissions. On the other hand, electricity demand during the peak period (19:00–21:45), identified based on the demand trend for this day from [40], is reduced by 93.2% in Case 1 and eliminated in Case 2. Since electricity prices and carbon emissions show a strong correlation (Fig. 5), reducing carbon emissions helps lower the electricity costs for EV charging. As shown in Table 4, incorporating CESS and MCSs reduces the electricity costs by intermittently charging during low-price periods and discharging during high-price periods. However, since the objective function in this study does not explicitly incorporate a term to minimize the electricity cost for EV charging, the costs calculated for Case 1 and Case 2 may not represent the optimal values. To enable a comprehensive cost-based comparison, an alternative objective function accounting for the investment and operational costs of the CESS, MCS, and FCSs should be considered, which might be the topic of a future study.

4. Additional Simulation Analyses

4.1 Scenario Analysis

In the scenario analysis, we considered a different test day—March 2, 2024—which falls in a different month and represents a weekend, in contrast to the previously analyzed day, April 30, 2024. This change impacts carbon emission variations throughout the day, EV charging demand, and the FCSs visited by EVs, based on data from April 30, 2024. For instance, the number of EVs requiring charging decreases from 126 to 100, while four new FCSs are visited, increasing the total number of FCSs from 13 to 14.

Figure 14 illustrates the variations in EV charging power sourced from the FCSs, CESS, and MCSs. The EV charging power supplied by FCSs increases during the day (08:00–19:00) due to reduced carbon emissions in this period, primarily driven by the

high number of PV installations at UC San Diego. On this day, 45.7% of the EV charging demand is met by CESS and MCSs, contributing to carbon emission reduction and reducing waiting times. The charging power of EVs results in 101.0 $kgCO_2$/day emissions on March 2, whereas it led to zero CO_2 emissions on April 30, as grid power did not contribute to carbon emissions during that period. On the other hand, if MCSs and energy storage technologies (MCSs and CESS) are omitted, as in the Base Case and Case 1, carbon emissions increase to 141.5 $kgCO_2$/day and 211.3 $kgCO_2$/day, respectively, on March 2. In addition, the total EV waiting time is 120 minutes in the Base Case and Case 1 but is eliminated in Case 2. These findings demonstrate that the proposed approach effectively reduces both carbon emissions and EV waiting times under different conditions.

4.2 Scalability Analysis

In the scalability analysis, we have examined three different communities to assess the extended impact of the proposed mechanism. We assumed that the data for one of these communities remained identical to that in the main cases. For the other two communities, we adjusted the number of EVs by approximately ±20%, resulting in 101 and 151 EVs visiting the FCSs across these communities. Table 5 presents the carbon emissions, EV waiting times, peak electricity demand, and total electricity costs for these additional communities. As observed in the table, these values are directly proportional to the charging demand of EVs. Moreover, when the number of EVs exceeded the system's capacity, as in Community-3, the FCSs struggled to accommodate the increased charging demand without significant delays. Even under these extreme conditions, the MCSs helped mitigate EV waiting times.

If these three communities are considered part of the same region, the large-scale impact of the proposed approach becomes evident in terms of carbon emissions, peak electricity demand, and total electricity costs. Specifically, the carbon emissions from EV charging are reduced by 90% and 55% compared to Base Case and Case 1, respectively. Similarly, the peak electricity demand is completely eliminated in Case 2, while the total electricity cost for EV charging decrease by 87% and 61% compared to Base Case and Case 1, respectively. It should be also noted that in this case, as the scale of the problem increased, computational cost grew due to the rising number of defined binary variables. To ensure computational feasibility in even larger-scale systems, it may be necessary to replace binary variables with linear variables to manage the computational cost effectively.

4.3 Comparative Analysis

To further assess the effectiveness of the proposed framework, we compared its results with those obtained from a scheduling method inspired by [42-43], which employs clustering techniques to optimize MCS dispatch. To ensure a fair and consistent comparison across these studies and our study, we assumed that in these studies where only MCSs were employed at predetermined locations, these locations functionally served as FCSs. This assumption enabled us to apply the new scheduling approach to our dataset of 126 EVs.

Table 5. Comparison of carbon emissions, waiting times, peak electricity demand, and electricity costs for communities.

		Carbon emission [$kgCO_2$/day]	EV waiting time [mins/day]	Peak electricity demand [kWh/day]	Total electricity cost [$/day]
Community-2 (101 EVs)	FCSs	73.2	30.0	113.8	15.8
	Case 1	8.8	30.0	0.0	2.5
	Case 2	8.7	0.0	0.0	2.5
Community-3 (151 EVs)	FCSs	132.3	1830.0	253.2	30.6
	Case 1	41.5	1830.0	115.4	12.6
	Case 2	11.5	135.0	0.0	3.3

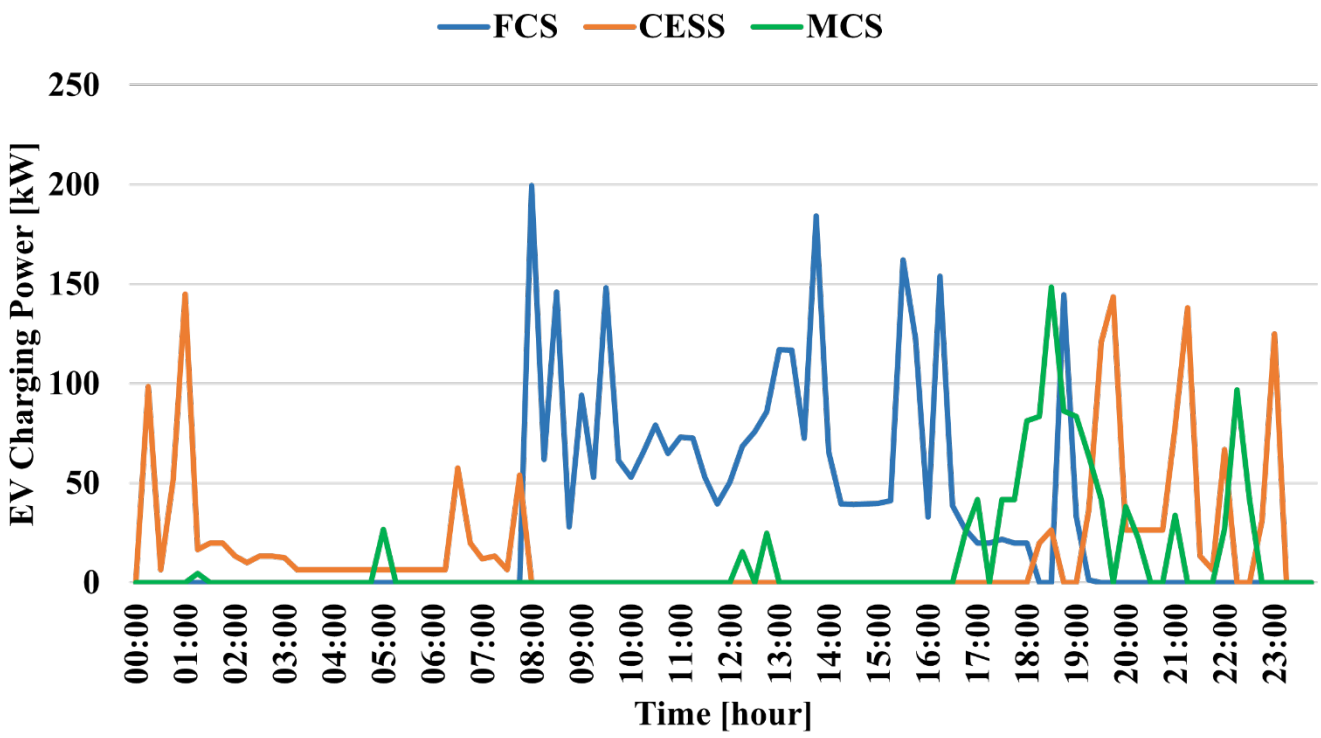


Fig. 14. EV charging power drawn from the FCS, CESS, and MCSs for Case 2 on March 2.

We clustered the nearest FCSs into five locations, maintaining the same total number of chargers across these FCSs. Additionally, we ensured methodological consistency by using the same number of MCSs and adopting an identical objective function. This standardization allowed for a precise and objective comparison of both approaches in terms of carbon emissions and waiting times.

Figure 15 compares the proposed model with the benchmark algorithm based on key parameters, including FCS utilization rate (the ratio of total power drawn by FCSs to total power drawn from the grid), carbon emissions, battery degradation cost, road consumption, and waiting time at FCSs. The figure illustrates that clustering EVs in specific locations increases energy consumption at FCSs. This occurs because the benchmark algorithm does not contain a CESS. Without the CESS, the MCSs have limited capacity to reduce energy consumption at FCSs and, consequently, carbon emissions. As a result, total carbon emissions are significantly higher for the clustering model, while battery degradation costs decrease slightly due to reduced battery utilization. The primary advantage of the benchmark algorithm is its ability to significantly lower the energy consumption of MCSs on the road, which aligns with the main objective of this algorithm. However, it does not affect EV waiting times. Consequently, the benchmark approach—where EVs charge at predetermined locations—may be beneficial in areas without FCSs. However, in areas with FCSs, directing EVs to specific locations may require users to deviate from their original routes, leading to additional time and energy losses. This could influence EV users' decisions, making them more likely to opt for nearby FCSs instead. Such shifts in user behavior may disrupt the coordination between FCSs and MCSs, ultimately increasing waiting times at FCSs.

4.4 Parameter Analysis

In this study, we combined multiple objectives, minimizing carbon emissions, waiting times, and battery degradation, into a single objective function by standardizing them as costs. To convert carbon emissions into a cost value, we used the social cost of carbon, estimated by the U.S. government at $50 per metric ton [41]. However, alternative values for the social cost of carbon have emerged in the literature, as the calculation depends on various subjective factors, including climate change projections and their economic impacts, such as changes in agricultural productivity, damage from sea level rise, and declines in human health.

To assess the impact of varying social cost values on optimization results, we conducted a parameter analysis and adopted a social cost of $185 per metric ton from [44]. Figure 16 clearly demonstrates that as the weight of carbon emissions increases in the objective function, total carbon emissions decrease by 64%, while battery degradation increases by 25% due to higher utilization of CESS and MCSs. A comprehensive economic assessment of the trade-off between battery utilization and carbon emission reduction is left for future studies.

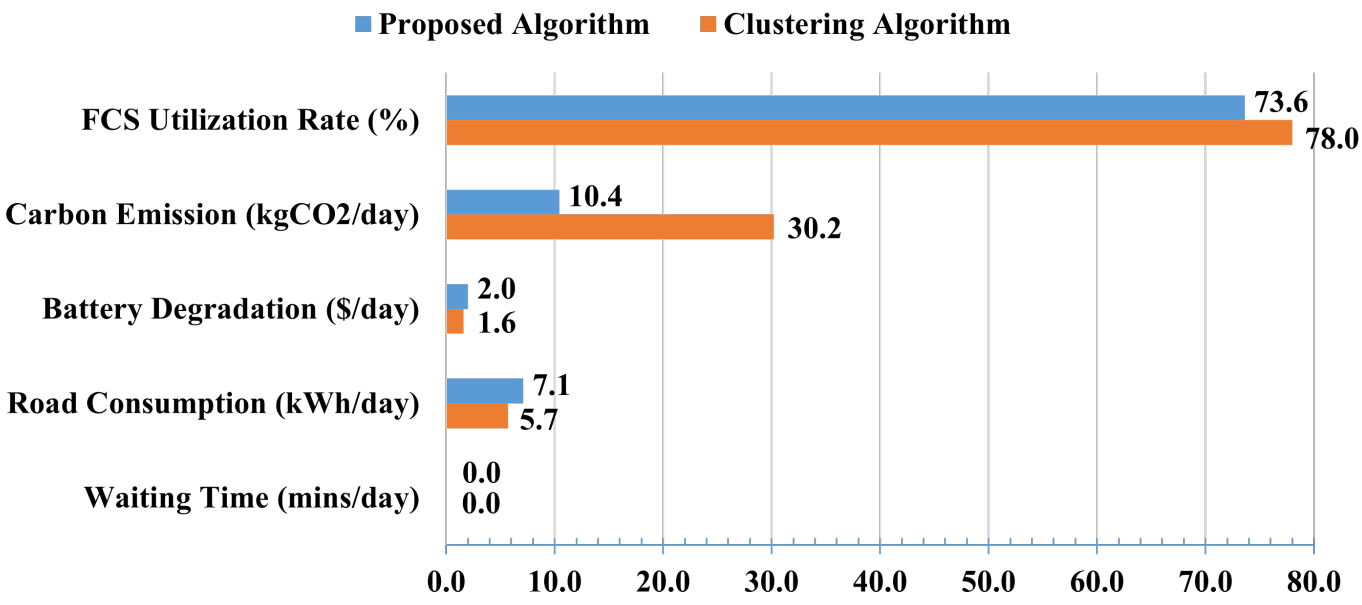


Fig. 15. Comparison of the proposed algorithm and the clustering algorithm based on [42-43].

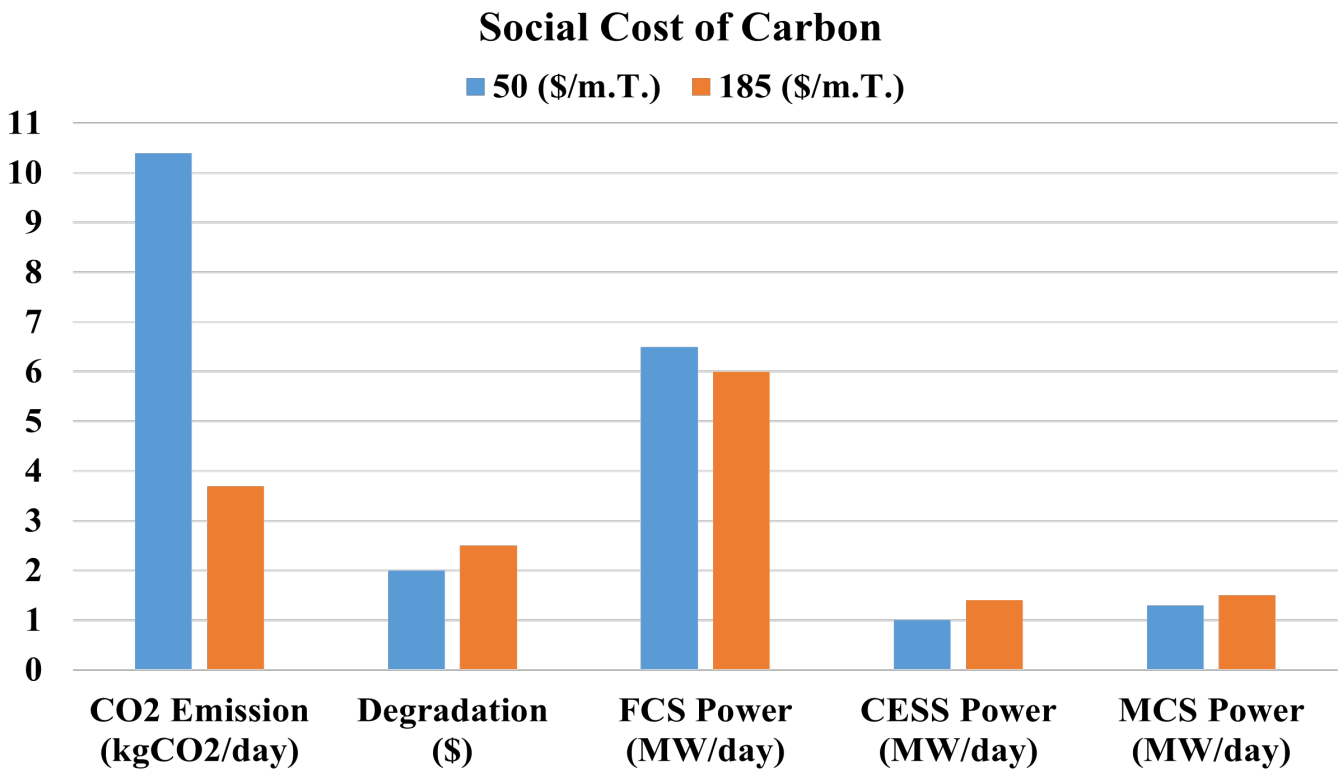


Fig. 16. Comparison of the main results based on variations in the social cost of carbon.

5. Discussion of MCS Opportunities

It is anticipated that over 1.1 million EV chargers will be required in California by 2035 to meet the demand of the transportation sector, which necessitates a $50 billion investment in distribution grid upgrades to meet the growing electricity demand [45]. Besides, EV charging loads are required to be flexible and shiftable to achieve zero-carbon electricity by 2045 [46]. To achieve a similar carbon net zero target by 2050, a free EV charging service is provided in Korea in power grids with a renewable energy ratio of over 80 percent [47]. These requirements and the other requirements defined by various government policies show the urgent need for alternative grid-independent charging solutions that may shift charging loads to grid-supportive locations and times, increase the renewable energy usage ratio in EV charging, and consider distribution grid conditions for charging operations.

MCSs can be effectively used for addressing all these targets without the constraints of location and time, particularly in densely populated cities, such as Los Angeles, Istanbul, Beijing, Tokyo and Delhi, where residential charging systems are not available to install due to parking space constraints [30]. With this objective, many companies such as Saniset Fleet [39], SparkCharge [48], EvoCharge [49], Blink Charging [50], and NIO Power [51], have recently developed and produced different types of MCSs. Among these companies, Saniset Fleet delivers up to 7.5 MWh of grid energy daily using electric trucks, offering flexible charging options and saving 136,000 kg of CO_2 [39]. In its first six months, SparkCharge completed over 1,500 charging deliveries, preventing 4.875 tons of CO_2 emissions. By May 2022, their service had provided over 100,000 miles of range, preventing more than 85 tons of CO_2 emissions [48]. Additionally, EvoCharge's MCS delivers up to 50 kW of power [49], while NIO Power's MCS offers up to 40 kW of power [51], enabling faster EV charging compared to standard Level 2 chargers and significantly reducing overall charging times. Driven by these benefits, the global MCS market is anticipated to be worth $63.2 million in 2025, with forecasts indicating it will expand to $388.9 million by 2035, supported by an average annual growth rate of 20.1% between 2026 and 2035 [52].

The real-world implementations and recent studies on MCSs have shown that the total cost of charging EVs using MCSs, including both investment and operational expenses, is slightly higher than charging with FCSs [17]. However, their unique advantages such as eliminating the waiting times at FCSs caused by limited charger availability or temporary unavailability, charging EVs even during working hours or night times, and reducing peak loads due to the simultaneous charging of many EVs make MCSs both a promising alternative and complimentary technology to FCSs. It is anticipated that the total cost of MCSs will be less than that of FCSs in the near future, given advancements in the battery technology and decrease in the areas suitable for FCSs.

6. Conclusions

This study proposes an optimal charging management strategy for EVs by coordinating a set of FCSs, MCSs, and a CESS. The study offers three key contributions to the current literature. First, MCSs are used together with existing FCSs to supply charging service for EVs with reduced carbon emissions and added user convenience. Second, a grid-connected CESS is integrated into the system to support EV charging with stored renewable energy and shifting of charging from the grid to low-emission times. Third, an optimization strategy is proposed to coordinate EV charging in a way that all the stakeholders can benefit while satisfying the EV operational requirements.

The performance of the proposed optimization framework is evaluated using comparisons with two different cases where only FCSs, and FCSs and a CESS are considered for EV charging. The most important findings are:

1. Compared with the two cases without the MCSs, the MCSs reduce the carbon emissions by 90% and 55%, respectively.
2. MCSs can eliminate the waiting times of EVs at FCSs, enhancing EV user experience, improving traffic flow around FCSs, reducing additional energy consumption and associated carbon emissions from idling, and decreasing the need for further FCS installations.
3. The load on the power grid is shifted to optimal times by the energy stored in the MCSs and CESS during off-peak periods.

It should be noted that the initial investment costs of MCSs and FCSs and the user acceptance of MCS have not been considered in the proposed optimization strategy. An in-depth analysis supported by survey and questionaries is required to address these impacts, which will be a topic for future work. Also, the EV charging session details were assumed to be perfectly known ahead of time, which simplifies the routing of MCSs. In reality, there is uncertainty in the timing, magnitude, and location of EV charging demand and modeling this uncertainty as well as mitigation strategies are left for future work. Lastly, incorporating a more advanced route optimization approach that accounts for traffic conditions and environmental variables would be a valuable direction for future research, particularly for larger geographical areas where MCSs are required to travel longer distances.

Acknowledgement

This work is supported by California Energy Commission - Energy Research Development Division under the award number GFO-23-306. The work of A. Taşcıkaraoğlu is supported by The Scientific and Technological Research Council of Turkey (TÜBİTAK) 2219 International Postdoctoral Research Fellowship Program, and also by the Turkish Academy of Sciences through the Distinguished Young Scientist Award Program. The authors thank Keaton Chia (University of California San Diego) for the provision of EV charging data.

Appendix A. Connection status constraints of EVs

Connection status constraints of the EVs are given by (A1-A12). First, it is important to note that certain time-dependent decisions, such as the connection of MCSs or the arrival and departure of EVs, occur at specific instants rather than over a continuous interval. To incorporate these instantaneous events into the optimization framework, we assume they occur at the beginning of the corresponding 15-minute time interval and represent them using a single time step. Equation (A1) guarantees that EV e can only be located at node i and charged at this node through either an FCS or an MCS. Constraints (A2) and (A3) determine the connection status of the EVs for FCSs and MCSs, respectively. The binary variables $\alpha_{e,t}^{\text{fx,start}}$ and $\alpha_{e,t}^{\text{mcs,start}}$ indicate whether charging has started within time interval t, while $\beta_{e,t}^{\text{fx,end}}$ and $\beta_{e,t}^{\text{mcs,end}}$ show whether the charging service has finished within time interval t. Therefore, one of the binary variables $y_{i,e,t}$ and $z_{i,e,t}$ takes a value of 1 during the charging process, depending on the charging method. Equation (A4) combines the charge starting indicators of FCSs and MCSs, ensuring that EVs are charged using one of the selected methods. The charging service cannot start before the EVs arrive at the nodes, as indicated in (A5).

Constraints (A6) and (A7) ensure that if EV e has been accepted for charging and the charging service has started, the service must end at a time within the optimization period. Equations (A8) to (A10) transform the binary variable $\alpha_{e,t}^{\text{tot,start}}$ into a positive variable $\mathfrak{T}_e^{\text{start}}$ that records the charging start time, using the order of each time period, ord_t, and a large positive number $\mathfrak{B}$. The binary operations in (A8) - (A10) are defined for linearization purposes. Equation (A11) calculates the charging start time of EV e, $\mathfrak{T}_e^{\text{start}}$, based on arrival time, $\mathfrak{T}_e^{\text{arr}}$, and waiting time, wt_e, while (A12) calculates the total waiting time.

$$z_{i,e,t} + y_{i,e,t} \leq \text{place}_{i,e}\,, z_{i,e,t} \in \{0,1\}, y_{i,e,t} \in \{0,1\}, \forall i \in N', \forall e \in E, \forall t \in T \tag{A1}$$

$$\alpha_{e,t}^{\text{fx,start}} - \beta_{e,t}^{\text{fx,end}} = \sum_{i \in N'} (y_{i,e,t} - y_{i,e,t-1}) \;, \alpha_{e,t}^{\text{fx,start}} \in \{0,1\}\,, \beta_{e,t}^{\text{fx,end}} \in \{0,1\}, y_{i,e,t} \in \{0,1\}\,, \forall e \in E, \forall t \in T \tag{A2}$$

$$\alpha_{e,t}^{\text{mcs,start}} - \beta_{e,t}^{\text{mcs,end}} = \sum_{i \in N'} \left(z_{i,e,t} - z_{i,e,t-1}\right), \alpha_{e,t}^{\text{mcs,start}} \in \{0,1\}\,, \beta_{e,t}^{\text{mcs,end}} \in \{0,1\}, z_{i,e,t} \in \{0,1\}\,, \forall e \in E, \forall t \in T \tag{A3}$$

$$\alpha_{e,t}^{\text{fx,start}} + \alpha_{e,t}^{\text{mcs,start}} = \alpha_{e,t}^{\text{tot,start}}, \alpha_{e,t}^{\text{fx,start}} \in \{0,1\}\,, \alpha_{e,t}^{\text{mcs,start}} \in \{0,1\}, \alpha_{e,t}^{\text{tot,start}} \in \{0,1\}\,, \forall e \in E, \forall t \in T \tag{A4}$$

$$\alpha_{e,t}^{\text{tot,start}} \leq \text{arr}_{e,t}^{\text{EV}},\ \alpha_{e,t}^{\text{tot,start}} \in \{0,1\}\,, \text{arr}_{e,t}^{\text{EV}} \in \{0,1\}\,, \forall e \in E, \forall t \in T \tag{A5}$$

$$\sum_{t \in T} \alpha_{e,t}^{\text{fx,start}} = \sum_{t \in T} \beta_{e,t}^{\text{fx,end}} \leq 1\,, \alpha_{e,t}^{\text{fx,start}} \in \{0,1\}\,, \beta_{e,t}^{\text{fx,end}} \in \{0,1\}\,, \forall e \in E \tag{A6}$$

$$\sum_{t \in T} \alpha_{e,t}^{\text{mcs,start}} = \sum_{t \in T} \beta_{e,t}^{\text{mcs,end}} \leq 1\,, \alpha_{e,t}^{\text{mcs,start}} \in \{0,1\}\,, \beta_{e,t}^{\text{mcs,end}} \in \{0,1\}\,, \forall e \in E \tag{A7}$$

$$\mathfrak{T}_e^{\text{start}} \leq \mathfrak{B} \cdot \alpha_{e,t}^{\text{tot,start}}, \alpha_{e,t}^{\text{tot,start}} \in \{0,1\}, \forall e \in E, \forall t \in T \tag{A8}$$

$$\mathfrak{T}_e^{\text{start}} \leq \text{ord}_t, \forall e \in E, \forall t \in T \tag{A9}$$

$$\mathfrak{T}_e^{\text{start}} \geq \text{ord}_t - \mathfrak{B} \cdot \left(1 - \alpha_{e,t}^{\text{tot,start}}\right), \alpha_{e,t}^{\text{tot,start}} \in \{0,1\}, \forall e \in E, \forall t \in T \tag{A10}$$

$$\mathfrak{T}_e^{\text{start}} = \mathfrak{T}_e^{\text{arr}} + \text{wt}_e, \forall e \in E \tag{A11}$$

$$\mathfrak{T}^{\text{wait}} = \sum_{e \in E} \text{wt}_e \cdot \Delta T \tag{A12}$$

Appendix B. Battery degradation rate

The battery degradation rates for CESS and MCSs, λ_{CESS}^{deg} and λ_{MCS}^{deg}, are calculated using the Arrhenius equation as shown in (B1), which is widely used to model battery aging [53-54], particularly for estimating how temperature influences battery degradation over time. In this equation, A represents the pre-exponential factor, determining how frequently degradation reactions occur, while E_a denotes the activation energy, representing the energy barrier for degradation. The term R corresponds to the universal gas constant (8.314 J/mol·K), and T is the absolute temperature in Kelvin, where higher temperatures accelerate degradation.

$$k = A \cdot e^{-\frac{E_a}{RT}} \tag{B1}$$

To account for additional factors including fast charging, high discharge rates and calendar aging, the degradation rate from the Arrhenius equation, k, can be modified as follows:

$$k_{eff} = k \cdot SF \tag{B2}$$

where k_{eff} is effective degradation rate and SF is stress factor accounting for real-world degradation effects. The total energy throughput over the battery's lifespan can be calculated as:

$$E_{total} = C_0 \cdot N_{cycle} \cdot DoD \cdot (1 - k_{eff}) \tag{B3}$$

where C_0 is initial battery capacity (kWh), N_{cycle} is cycle life, and DoD is depth of discharge. The total cost of battery aging accounts for the effective cost after considering salvage value:

$$C_{eff} = C_{battery} \cdot (1 - SV) \tag{B4}$$

where $C_{battery}$ is battery cost per kWh ($/kWh) and SV is salvage value. Finally, the cost per kWh cycled is:

$$\lambda^{deg} = \frac{C_{eff}}{E_{total}} \tag{B5}$$

Appendix C. MCS operation constraints

Connection status constraints of the MCSs are given by (C1)-(C8). Equation (C1) establishes flow consistency, ensuring that the number of arrivals at node i for MCS m is equal to the number of departures from node i. In other words, when MCS m visits a node, it must arrive at the node and then depart from it. The binary variable $x_{m,i,j,t}$ indicates whether MCS m travels from node i to node j. The spatio-temporal status of the MCSs is represented by binary variables $\delta_{m,i,t}^{\mathrm{mcs,arr}}$, $\mu_{m,i,t}^{\mathrm{mcs,dep}}$, $\kappa_{m,i,t}$ and $x_{m,i,j,t}$, which collectively describe the movement and connectivity of MCSs over time. The binary variable $\delta_{m,i,t}^{\mathrm{mcs,arr}}$ is assigned a value of 1 if MCS m arrives at node i during time period t. Similarly, the binary variable $\mu_{m,i,t}^{\mathrm{mcs,dep}}$ takes a value of 1 if MCS m departs from node i at time t, ensuring clear tracking of its arrival and departure activities. Hence, the connection status of MCS m at node i in time period t is captured by $\kappa_{m,i,t}$ which is determined based on the arrival and departure times, as formulated in Equation (C2). Equation (C3) enforces a fundamental constraint, ensuring that an MCS can be connected to only one node during a given time period. Constraint (C4) guarantees that an MCS departs from node i at time t and subsequently arrives at node j at time tt, modeling its mobility between different locations. The binary variable $x_{m,j,i,t}$ is defined to be 1 when MCS m reaches node j at time t. Additionally, Equation (C6) prevents MCSs from arriving at and departing from the same node within the same time period, thereby avoiding redundant and conflicting states in the model. To optimize traffic flow and minimize congestion, constraints (C7) and (C8) limit each MCS to visiting FCS nodes only once per day. This restriction is particularly important in areas with limited infrastructure, such as university campuses and narrow urban streets, where frequent movements of large MCSs could lead to operational inefficiencies and logistical challenges.

$$\sum_{j\in N,t\in T} x_{m,i,j,t} = \sum_{j\in N,t\in T} x_{m,j,i,t}\ , x_{m,i,j,t} \in \{0,1\}, \forall i \in N, \forall (i,j) \in R \tag{C1}$$

$$\delta_{m,i,t}^{\mathrm{mcs,arr}} - \mu_{m,i,t}^{\mathrm{mcs,dep}} = \kappa_{m,i,t} - \kappa_{m,i,t-1}\ , \delta_{m,i,t}^{\mathrm{mcs,arr}} \in \{0,1\}, \mu_{m,i,t}^{\mathrm{mcs,dep}} \in \{0,1\}, \kappa_{m,i,t} \in \{0,1\}, \forall m \in M, \forall i \in N, \text{if } t \neq t^0 \tag{C2}$$

$$\sum_{i\in N} \kappa_{m,i,t} \leq 1\ , \kappa_{m,i,t} \in \{0,1\}, \forall m \in M, \forall t \in T \tag{C3}$$

$$x_{m,i,j,tt} \leq \mu_{m,i,t}^{\mathrm{mcs,dep}}, x_{m,i,j,tt} \in \{0,1\}, \forall m \in M, \forall (i,j) \in R, \forall tt \geq t + \mathcal{T}_{i,j}^{\mathrm{way}} \tag{C4}$$

$$\delta_{m,j,t}^{\mathrm{mcs,arr}} = \sum_{i\in N} x_{m,i,j,t}\ , \delta_{m,j,t}^{\mathrm{mcs,arr}} \in \{0,1\}, x_{m,i,j,t} \in \{0,1\}, \forall m \in M, \forall (i,j) \in R, \forall t \in T \tag{C5}$$

$$\delta_{m,i,t}^{\mathrm{mcs,arr}} + \mu_{m,i,t}^{\mathrm{mcs,dep}} \leq 1\ , \delta_{m,i,t}^{\mathrm{mcs,arr}} \in \{0,1\}\ , \mu_{m,i,t}^{\mathrm{mcs,dep}} \in \{0,1\}, \forall m \in M, \forall i \in N, \forall t \in T \tag{C6}$$

$$\sum_{t\in T} \delta_{m,i,t}^{\mathrm{mcs,arr}} \leq 1\ , \delta_{m,i,t}^{\mathrm{mcs,arr}} \in \{0,1\}, \forall m \in M, \forall i \in N' \tag{C7}$$

$$\sum_{t\in T} \mu_{m,i,t}^{\mathrm{mcs,dep}} \leq 1\ , \mu_{m,i,t}^{\mathrm{mcs,dep}} \in \{0,1\}, \forall m \in M, \forall i \in N' \tag{C8}$$

References

[1] International Energy Agency (IEA), "Greenhouse Gas Emissions From Energy Highlights," 2021.

[2] W. Guedes, C. Oliveira, T. A. Soares, B. H. Dias, and M. Matos, "Collective Asset Sharing Mechanisms for PV and BESS in Renewable Energy Communities," *IEEE Trans Smart Grid*, vol. 15, no. 1, pp. 607–616, 2024, doi: 10.1109/TSG.2023.3288533.

[3] J.-W. Xiao, Y.-B. Yang, S. Cui, and X.-K. Liu, "A new energy storage sharing framework with regard to both storage capacity and power capacity," *Appl Energy*, vol. 307, p. 118171, 2022, doi: https://doi.org/10.1016/j.apenergy.2021.118171.

[4] Y. Zabihinia Gerdroodbari, M. Khorasany, R. Razzaghi, and R. Heidari, "Management of prosumers using dynamic export limits and shared Community Energy Storage," *Appl Energy*, vol. 355, p. 122222, 2024, doi: https://doi.org/10.1016/j.apenergy.2023.122222.

[5] N. Pei, X. Song, Z. Zhang, and F. Peña-Mora, "Optimizing the operation and allocating the cost of shared energy storage for multiple renewable energy stations in power generation side," *Energy Convers Manag*, vol. 302, p. 118148, 2024, doi: https://doi.org/10.1016/j.enconman.2024.118148.

[6] L. Li, K. Peng, X. Yang, and K. Liu, "Coordinated design of multi-stakeholder community energy systems and shared energy storage under uncertain supply and demand: A game theoretical approach," *Sustain Cities Soc*, vol. 100, p. 105028, 2024, doi: https://doi.org/10.1016/j.scs.2023.105028.

[7] K. Berg, A. Hernandez-Matheus, M. Aragüés-Peñalba, E. Bullich-Massagué, and H. Farahmand, "Load configuration impact on energy community and distribution grid: Quantifying costs, emissions and grid exchange," *Appl Energy*, vol. 363, p. 123060, 2024, doi: https://doi.org/10.1016/j.apenergy.2024.123060.

[8] Md. M. Alam, R. Bin Mofidul, and Y. M. Jang, "Community energy storage system: Deep learning based optimal energy management solution for residential community," *J Energy Storage*, vol. 64, p. 107100, 2023, doi: https://doi.org/10.1016/j.est.2023.107100.

[9] H. Ghasemnejad, M. Rashidinejad, A. Abdollahi, and S. Dorahaki, "Energy management in citizen energy communities: A flexibility-constrained robust optimization approach considering prosumers comfort," *Appl Energy*, vol. 356, p. 122456, 2024, doi: https://doi.org/10.1016/j.apenergy.2023.122456.

[10] K. B. J. Anuradha, J. Iria, and C. P. Mediwaththe, "Multi-objective planning of community energy storage systems under uncertainty," *Electric Power Systems Research*, vol. 230, p. 110286, 2024, doi: https://doi.org/10.1016/j.epsr.2024.110286.

[11] S. Dorahaki, M. Rashidinejad, M. MollahassaniPour, M. Pourakbari Kasmaei, and P. Afzali, "A sharing economy model for a sustainable community energy storage considering end-user comfort," *Sustain Cities Soc*, vol. 97, p. 104786, 2023, doi: https://doi.org/10.1016/j.scs.2023.104786.

[12] B. Gu *et al.*, "A data-driven stochastic energy sharing optimization and implementation for community energy storage and PV prosumers," *Sustainable Energy, Grids and Networks*, vol. 34, p. 101051, 2023, doi: https://doi.org/10.1016/j.segan.2023.101051.

[13] M. Houwing, I. Dukovska, and N. G. Paterakis, "A Reputation Management System for the Fair Utilization of Community Energy Storage Systems," *IEEE Trans Smart Grid*, vol. 14, no. 1, pp. 582–592, 2023, doi: 10.1109/TSG.2022.3197355.

[14] B. Hudson, G. Razeghi, and S. Samuelsen, "Mitigating impacts associated with a high-penetration of plug-in electric vehicles on local residential smart grid infrastructure," *J Power Sources*, vol. 593, p. 233961, 2024, doi: https://doi.org/10.1016/j.jpowsour.2023.233961.

[15] K. Berg, R. Rana, and H. Farahmand, "Quantifying the benefits of shared battery in a DSO-energy community cooperation," *Appl Energy*, vol. 343, p. 121105, 2023, doi: https://doi.org/10.1016/j.apenergy.2023.121105.

[16] S. Cho, J. Lim, W. Won, J. Kim, and S. Ga, "Design and optimization of energy supplying system for electric vehicles by mobile charge stations," *Journal of Industrial and Engineering Chemistry*, vol. 138, pp. 481–491, 2024, doi: https://doi.org/10.1016/j.jiec.2024.04.027.

[17] U. Qureshi, A. Ghosh, and B. K. Panigrahi, "Scheduling and Routing of Mobile Charging Stations With Stochastic Travel Times to Service Heterogeneous Spatiotemporal Electric Vehicle Charging Requests With Time Windows," *IEEE Trans Ind Appl*, vol. 58, no. 5, pp. 6546–6556, 2022, doi: 10.1109/TIA.2022.3182323.

[18] M. E. Kabir, I. Sorkhoh, B. Moussa, and C. Assi, "Joint Routing and Scheduling of Mobile Charging Infrastructure for V2V Energy Transfer," *IEEE Transactions on Intelligent Vehicles*, vol. 6, no. 4, pp. 736–746, 2021, doi: 10.1109/TIV.2021.3063221.

[19] H. Li, D. Son, and B. Jeong, "Electric vehicle charging scheduling with mobile charging stations," *J Clean Prod*, vol. 434, p. 140162, 2024, doi: https://doi.org/10.1016/j.jclepro.2023.140162.

[20] P. Tang, F. He, X. Lin, and M. Li, "Online-to-offline mobile charging system for electric vehicles: Strategic planning and online operation," *Transp Res D Transp Environ*, vol. 87, p. 102522, 2020, doi: https://doi.org/10.1016/j.trd.2020.102522.

[21] Z. Zhang, Z. Y. Dong, and C. Yip, "A New Charging Scheme Based on Mobile Charging Robots Cluster: A Three-Level Coordinated Perspective," *IEEE Trans Industr Inform*, vol. 20, no. 4, pp. 6900–6912, 2024, doi: 10.1109/TII.2024.3352182.

[22] L. Liu, S. Liu, J. Wu, and J. Xu, "A Placement Strategy for Idle Mobile Charging Stations in IoEV: From the View of Charging Demand Force," *IEEE Transactions on Intelligent Transportation Systems*, vol. 25, no. 5, pp. 3870–3884, 2024, doi: 10.1109/TITS.2023.3329453.

[23] L. Liu, X. Qi, Z. Xi, J. Wu, and J. Xu, "Charging-Expense Minimization Through Assignment Rescheduling of Movable Charging Stations in Electric Vehicle Networks," *IEEE Transactions on Intelligent Transportation Systems*, vol. 23, no. 10, pp. 17212–17223, 2022, doi: 10.1109/TITS.2022.3154444.

[24] L. Liu, Z. Xi, K. Zhu, R. Wang, and E. Hossain, "Mobile Charging Station Placements in Internet of Electric Vehicles: A Federated Learning Approach," *IEEE Transactions on Intelligent Transportation Systems*, vol. 23, no. 12, pp. 24561–24577, 2022, doi: 10.1109/TITS.2022.3205596.

[25] L. Liu, H. Zhang, J. Xu, and P. Wang, "Providing Active Charging Services: An Assignment Strategy With Profit-Maximizing Heat Maps for Idle Mobile Charging Stations," *IEEE Trans Mob Comput*, vol. 23, no. 3, pp. 2139–2152, 2024, doi: 10.1109/TMC.2023.3247441.

[26] M. Nazari-Heris, A. Loni, S. Asadi, and B. Mohammadi-ivatloo, "Toward social equity access and mobile charging stations for electric vehicles: A case study in Los Angeles," *Appl Energy*, vol. 311, p. 118704, 2022, doi: https://doi.org/10.1016/j.apenergy.2022.118704.

[27] L. Hou, O. E. Herrera, and W. Mérida, "Charging scheduling and energy management for mobile chargers in a grid-interactive transportation system," *J Energy Storage*, vol. 65, p. 107305, 2023, doi: https://doi.org/10.1016/j.est.2023.107305.

[28] S. Afshar, Z. K. Pecenak, M. Barati, and V. Disfani, "Mobile charging stations for EV charging management in urban areas: A case study in Chattanooga," *Appl Energy*, vol. 325, p. 119901, 2022, doi: https://doi.org/10.1016/j.apenergy.2022.119901.

[29] M. A. Beyazıt and A. Taşcıkaraoğlu, "Electric vehicle charging through mobile charging station deployment in coupled distribution and transportation networks," *Sustainable Energy, Grids and Networks*, vol. 35, p. 101102, 2023, doi: https://doi.org/10.1016/j.segan.2023.101102.

[30] A. K. Aktar, A. Taşcıkaraoğlu, and J. P. S. Catalão, "Scheduling of mobile charging stations with local renewable energy sources," *Sustainable Energy, Grids and Networks*, vol. 37, p. 101257, 2024, doi: https://doi.org/10.1016/j.segan.2023.101257.

[31] M. A. Beyazit, A. K. Erenoglu, and A. Tascikaraoglu, "Fairness and Equity in Electric Vehicle Charging With Mobile Charging Stations," *IEEE Trans Ind Appl*, vol. 61, no. 1, pp. 1280–1291, 2025, doi: 10.1109/TIA.2024.3477426.

[32] A. C. Erüst, M. A. Beyazıt, F. Y. Taşcıkaraoğlu, and A. Taşcıkaraoğlu, "Deep Reinforcement Learning-Based Navigation Strategy for a Mobile Charging Station in a Dynamic Environment," in *2023 International Conference on Smart Energy Systems and Technologies (SEST)*, 2023, pp. 1–6. doi: 10.1109/SEST57387.2023.10257478.

[33] Y.-A. Chen, W. Zeng, A. Khurram, and J. Kleissl, "Cost-Optimal Aggregated Electric Vehicle Flexibility for Demand Response Market Participation by Workplace Electric Vehicle Charging Aggregators," *Energies (Basel)*, vol. 17, no. 7, 2024, doi: 10.3390/en17071745.

[34] "Tesla Owners Manual." Accessed: Mar. 18, 2025. [Online]. Available: https://www.tesla.com/ownersmanual/2015_2020_modelx/en_ie/GUID-BEE08D47-0CE0-4BDD-83F2-9854FB3D578F.html

[35] "Hyundai Kona-Electric." Accessed: Mar. 18, 2025. [Online]. Available: https://www.hyundai.com/ng/en/find-a-car/kona-electric/performance

[36] "NREL." Accessed: Mar. 18, 2025. [Online]. Available: https://www.nrel.gov/docs/fy22osti/83586.pdf

[37] J. Wang, Q. Guo, H. Sun, and M. Chen, "Collaborative optimization of logistics and electricity for the mobile charging service system," *Appl Energy*, vol. 336, p. 120845, 2023, doi: https://doi.org/10.1016/j.apenergy.2023.120845.

[38] B. Çatay and İ. Sadati, "An improved matheuristic for solving the electric vehicle routing problem with time windows and synchronized mobile charging/battery swapping," *Comput Oper Res*, vol. 159, p. 106310, 2023, doi: https://doi.org/10.1016/j.cor.2023.106310.

[39] "Saniset Fleet." Accessed: Dec. 20, 2024. [Online]. Available: https://www.sanisetfleet.com/mobile-battery/

[40] "California Independent System Operator (CAISO)." Accessed: Dec. 20, 2024. [Online]. Available: https://www.caiso.com/todays-outlook/

[41] K.-W. Cheng, Y. Bian, Y. Shi, and Y. Chen, "Carbon-Aware EV Charging," in *2022 IEEE International Conference on Communications, Control, and Computing Technologies for Smart Grids (SmartGridComm)*, 2022, pp. 186–192. doi: 10.1109/SmartGridComm52983.2022.9960988.

[42] K. G. Firouzjah and J. Ghasemi, "A clustering-based approach to scenario-driven planning for EV charging with autonomous mobile chargers," *Appl Energy*, vol. 379, p. 124925, 2025, doi: https://doi.org/10.1016/j.apenergy.2024.124925.

[43] H. Li, D. Son, and B. Jeong, "Electric vehicle charging scheduling with mobile charging stations," *J Clean Prod*, vol. 434, p. 140162, 2024, doi: https://doi.org/10.1016/j.jclepro.2023.140162.

[44] K. Rennert *et al.*, "Comprehensive evidence implies a higher social cost of CO2," *Nature*, vol. 610, no. 7933, pp. 687–692, 2022, doi: 10.1038/s41586-022-05224-9.

[45] “Electrification impacts study (2023),” Kevala. Accessed: Dec. 20, 2024. [Online]. Available: https://docs.cpuc.ca.gov/PublishedDocs/Efile/G000/M508/K423/508423247.pdf
[46] “Integrated Energy Policy Report Committee (2023).” Accessed: Mar. 18, 2025. [Online]. Available: https://www.energy.ca.gov/data-reports/reports/integrated-energy-policy-report-iepr/2023-integrated-energy-policy-report
[47] “2050 Neutrality Scenario [in Korean], 2021.” Accessed: Dec. 20, 2024. [Online]. Available: https://www.2050cnc.go.kr/base/board/read?boardManagementNo=4&boardNo=101&searchCategory=&page=1&searchType=&searchWord=&menuLevel=2&menuNo=15
[48] “SparkCharge Mobile Electric Vehicle Charging Service Provider.” Accessed: Jul. 23, 2024. [Online]. Available: https://www.sparkcharge.io/
[49] “EvoCharge Mobile DC Fast Power Station.” Accessed: Dec. 20, 2024. [Online]. Available: https://commercial.evocharge.com/product/evocharge-mobile-dc-fast-power-station
[50] “Blink Mobile EV Charging Service.” Accessed: Jul. 23, 2024. [Online]. Available: https://blinkcharging.com/products/mobile-charger
[51] “Nio Power Mobile.” Accessed: Jul. 23, 2024. [Online]. Available: https://www.nio.com/nio-power
[52] “Allied Market Research, Portable EV charger market: Global opportunity analysis and industry forecast, 2025-2035.” Accessed: Mar. 18, 2025. [Online]. Available: https://www.alliedmarketresearch.com/portable-ev-charger-market-A47223
[53] M. A. Bamdezh and G. R. Molaeimanesh, “The effect of active and passive battery thermal management systems on energy consumption, battery degradation, and carbon emissions of an electric vehicle,” *Energy*, vol. 304, p. 132134, 2024, doi: https://doi.org/10.1016/j.energy.2024.132134.
[54] M. Feinauer, M. Wohlfahrt-Mehrens, M. Hölzle, and T. Waldmann, “Temperature-driven path dependence in Li-ion battery cyclic aging,” *J Power Sources*, vol. 594, p. 233948, 2024, doi: https://doi.org/10.1016/j.jpowsour.2023.233948.